A

Appendix A: Technical Appendix

Local Risk Assessments

As part of the hazard identification and risk assessment process, the planning team reviewed parish plans to identify profiled hazards that were consistent with the State Hazard Mitigation Plan Committee's (SHMPC's) evaluation of the most serious natural hazard threats to the state. Some hazards identified in parish and municipal plans are not addressed directly in this plan update. Generally, these hazards appear in a small number of parish and municipal plans and were not consistent with the SHMPC's evaluation of the most serious natural hazard threats to the state.

Members from the SHMPC and the LSU Advisory Team reviewed each of the 60 available most up-to-date parish plans in the state to identify the hazards profiled in each plan in order to determine (1) the frequency with which each was addressed, and (2) whether sufficient consistency between the local plans exists to integrate the data, methods, and results systematically into the plan update.

The following table lists the hazards profiled in the available 60 parish plans for each of the hazards (or sub-hazards) included in this plan update. The hazard most often addressed by parish plans was tropical cyclones, which appeared in all the parishes for hazard profiling. Sinkhole hazard was addressed by 17 parish plans, and only two parish plans profiled sea level rise as a hazard. Parish plans included an average of 9 of the 21 hazards (or sub-hazards) included in this plan update. The Avoyelles Parish plan considers the fewest hazards profiled in this plan update (4 hazards), while three parish plans (East Baton Rouge, Jefferson, and Red River) considered 12 or more from among the 22 hazards profiled in this plan update.

Overall, the parish plans and the state plan update were found to be consistent in identifying natural hazards that impact areas of the state. Although the identified hazards are largely consistent, the parish plans vary widely in key characteristics, including hazard identification definitions, risk assessment data, risk assessment methodologies, and economic loss estimation. The primary commonality among the plans is the inclusion of Hazus Level 1 analyses. This update includes Level 1 flood, wind, and combined wind and flood model results. Thus, the risk assessments for these prevalent hazards are consistent among the parish and state plans.

	La Salle	Jefferson Davis	Jefferson	Jackson	Iberville	Iberia	Grant	Franklin	Evangeline	East Feliciana	East Carroll	East Baton Rouge	DeSoto	Concordia	Claiborne	Catahoula	Cameron	Caldwell	Caddo	Bossier	Bienville	Beauregard	Avoyelles	Assumption	Ascension	Acadia
Subsidence			X		X	X				*		*													X	
Land Loss					X	X						*					X									
Coastal Erosion			X																							
Saltwater Intrusion						X																				
Sea Level Rise						X																				
Drought	X	X	X			*	X	X	X	X	X	X	X	X	X	X	X	X	X	X	X	X				X
Earthquake			X									*	*	*	*				*	*						
Flooding	X	X	X	X	X	X	X	X	X	X	X	X	X	X	X	X	X	X	X	X	X	X	X	X	X	X
Extreme Heat			X					X					X	X	X		X		X		X	X				
Thunderstorms	X	X	X	X	X	X	X	X	X	X	X	X	X	X	X	X	X	X	X	X	X	X	X	X	X	X
Tornadoes	X	X	X	X	X	X	X	X	X	X	X	X	X	X	X	X	X	X	X	X	X	X	X	X	X	X
Tropical Cyclones	X	X	X	X	X	X	X	X	X	X	X	X	X	X	X	X	X	X	X	X	X	X	X	X	X	X
Wildfires	X	X	X				X			X	X	X	X	X	X		X	X	X	X	X	X				
Winter Storms	X	X	X				X	X	X	X	X	X	X	X	X	X		X	X	X	X	X		X	X	X
Dam Failure				+				X	+	+		+	*	+	+			+	+	+	X					
Levee Failure		X		+	X	X	X	+		+	X	+	*	+	+			+	+	+					X	
Sinkholes						X		X	X								X					X		X	X	
Storm Surge			X																							
Fog																										
Expansive Soil																										
Hailstorms			X																							
Hazardous Materials																										

	Union	Terrebonne	Tensas	Tangipahoa	St. Tammany	St. Mary	St. Martin	St. Landry	St. John the Baptist	St. James	St. Helena	St. Charles	St. Bernard	Sabine	Richland	Red River	Rapides	Point Coupee	Plaquemines	Ouachita	Orleans	Natchitoches	Morehouse	Madison	Livingston	Lincoln
Subsidence		X		X			X			X			X			X			X		X				X	
Land Loss				X	X							X				X					X				X	
Coastal Erosion		X				X						X														
Saltwater Intrusion		X										X	X						X							
Sea Level Rise																			X							
Drought	X		X		X	X	X	X	X	X				X	X	X	X	X		X		X	X		X	X
Earthquake	*		*													*				*						*
Flooding	X	X	X	X	X	X	X	X	X	X	X		X	X	X	X	X	X	X	X	X	X	X	X	X	X
Extreme Heat	X	X	X													X	X			X	X		X			X
Thunderstorms	X	X	X	X	X	X		X	X	X	X		X	X	X	X	X	X	X	X	X	X	X	X	X	X
Tornadoes	X	X	X	X	X	X	X	X	X	X	X		X	X	X	X	X	X	X	X	X	X	X	X	X	X
Tropical Cyclones	X	X	X	X	X	X	X	X	X	X	X	X	X	X	X	X	X	X	X	X	X	X	X	X	X	X
Wildfires	X		X	X	X			X		X	X			X		X	X			X		X	X			X
Winter Storms	X		X	X		X		X	X	X	X	X		X	X	X	X	X		X	X	X	X	X	X	X
Dam Failure	+				X									+	+	+		+		+	X		+			+
Levee Failure	+	X	X		X		X					X			*	+		+	X	+	X		+	+		
Sinkholes		X	X							X			X						X					X		
Storm Surge																					X					
Fog					X																					
Expansive Soil							X		X	X						*										
Hailstorms							X																		X	
Hazardous Materials												X														

	Vermilion	Vernon	Washington	Webster	West Baton Rouge	West Carroll	West Feliciana	Winn
Subsidence					*			
Land Loss	X				*			
Coastal Erosion								
Saltwater Intrusion								
Sea Level Rise								
Drought		X		X	X	X		X
Earthquake		*						
Flooding	X	X	X	X	X	X	X	X
Extreme Heat		X		X				
Thunderstorms	X	X	X	X	X	X	X	X
Tornadoes	X	X	X	X	X	X	X	X
Tropical Cyclones	X	X	X	X	X	X	X	X
Wildfires		X	X	X	X		X	X
Winter Storms		X	X	X	X	X		
Dam Failure		+		X			X	
Levee Failure		+					X	
Sinkholes	X			X	X			X
Storm Surge								
Fog								
Expansive Soil								
Hailstorms								
Hazardous Materials								

X - Hazard Profiled

* - Hazard Profiled but Discounted

+ - Hazard Profiled but Data Deficiency

Most of the recent updates to jurisdictional plans follow the general methodology of the 2014 and 2019 State Hazard Mitigation Plans. This plan update utilizes data from the Spatial Hazard Events and Losses Database for the United States (SHELDUS). This is considered an improvement over parish plan data, as SHELDUS integrates data from National Centers for Environmental Information with additional data from the NOAA Storm Prediction Center, National Hurricane Center, and U.S. Fire Administration. Additionally, data from multiple state agencies have been integrated into the current plan.

Changes in Development

Parish-level population

Future population estimations were calculated at the census block level of each Louisiana parish for 2050. Annual estimates and census data were obtained from U.S. Census Bureau for each parish. The file consists of yearly population estimates (Pyear) for each parish from 1981 to 2020. These population estimates are used to calculate how the population changed from the previous year up until 2020 for each parish. The overall average rate (r) of population change was calculated based of the 40 annual population changes determined for each parish (Equation 1).

Average population change from 1980 to 2020

$$r = \left(\frac{(P_{1981} - P_{1980})}{P_{1980}} + \frac{(P_{1982} - P_{1981})}{P_{1981}} + \ldots\ldots + \frac{(P_{2020} - P_{2019})}{P_{2019}} \right) / 40 \quad \text{(Equation 1)}$$

After the average annual population rate (r) was determined, future population estimates (Pf) for each Louisiana parish at the census block level were calculated for 2050 (Equation 2). The 2020 block level U.S. Census population data (Po) was used as the initial base to estimate how the future population Louisiana changed during the 30-year period (t).

$$P_f = P_0 e^{rt} \quad \text{(Equation 2)}$$

The following table presents the parish-level population results.

Parish	Population 2020	Population 2050	Projected Change
Acadia	57,576	56,738	(838)
Allen	22,750	19,850	(2,900)
Ascension	126,500	264,000	137,500
Assumption	21,039	17,998	(3,041)
Avoyelles	39,693	36,316	(3,377)
Beauregard	36,549	42,796	6,247
Bienville	12,981	9,636	(3,345)
Bossier	128,746	183,717	54,971
Caddo	237,848	209,827	(28,021)
Calcasieu	216,785	239,947	23,162
Caldwell	9,645	8,519	(1,126)
Cameron	5,617	2,392	(3,225)
Catahoula	8,906	6,538	(2,368)
Claiborne	14,170	11,205	(2,965)
Concordia	18,687	16,257	(2,430)
DeSoto	26,812	29,193	2,381
East Baton Rouge	456,781	509,869	53,088
East Carroll	7,459	4,863	(2,596)
East Feliciana	19,539	16,726	(2,813)
Evangeline	32,350	28,432	(3,918)
Franklin	19,774	17,447	(2,327)
Grant	22,169	27,900	5,731
Iberia	69,929	63,160	(6,769)
Iberville	30,241	26,211	(4,030)
Jackson	15,031	14,554	(477)
Jefferson	440,781	400,031	(40,750)
Jefferson Davis	32,250	32,858	608
Lafayette	241,753	350,331	108,578

Lafourche	97,557	106,639	9,082
LaSalle	14,791	15,529	738
Lincoln	48,396	56,799	8,403
Livingston	142,282	276,258	133,976
Madison	10,017	6,325	(3,692)
Morehouse	25,629	18,331	(7,298)
Natchitoches	37,515	34,650	(2,865)
Orleans	383,997	379,918	(4,079)
Ouachita	160,368	173,360	12,992
Plaquemines	23,515	19,412	(4,103)
Pointe Coupee	20,758	17,818	(2,940)
Rapides	130,023	130,521	498
Red River	7,620	5,546	(2,074)
Richland	20,043	18,550	(1,493)
Sabine	22,155	20,907	(1,248)
St. Bernard	43,764	78,104	34,340
St. Charles	52,549	57,309	4,760
St. Helena	10,920	11,154	234
St. James	20,192	18,100	(2,092)
St. John the Baptist	42,477	38,169	(4,308)
St. Landry	82,540	75,047	(7,493)
St. Martin	51,767	56,138	4,371
St. Mary	49,406	42,249	(7,157)
St. Tammany	264,570	431,427	166,857
Tangipahoa	133,157	206,004	72,847
Tensas	4,147	1,988	(2,159)
Terrebonne	109,580	109,756	176

Union	21,107	18,838	(2,269)
Vermilion	57,359	62,567	5,208
Vernon	48,750	42,766	(5,984)
Washington	45,463	47,077	1,614
Webster	36,967	29,980	(6,987)
West Baton Rouge	27,199	39,028	11,829
West Carroll	9,751	7,150	(2,601)

The latest six National Land Cover Databases (NLCD) are used to describe how the urban land cover across Louisiana has changed between 2001, 2006, 2011, 2016, 2019, and 2021. A description of the data sets used in the analysis is readily available and stated below from NLCD (https://www.mrlc.gov/data).

National Land Cover Database 2021 (NLCD 2021) is the most recent national land cover product created by the Multi-Resolution Land Characteristics (MRLC) Consortium. NLCD 2021 builds upon the foundation of NLCD 2016, and it follows an update-based approach where certain products, such as Land Cover and Impervious Surface, remain unchanged from the 2019 release. These unchanged products are utilized directly with NLCD 2021 for change analysis over the specified time span. However, it is noted that science products and the change index have been updated to incorporate additional changes observed in 2021. Therefore, users interested in the most recent and comprehensive analysis of land cover changes during the NLCD timespan would need to acquire the updated science products and change index for NLCD 2021. This approach ensures that the data set reflects the latest developments in land cover and impervious surface changes, providing researchers and practitioners with accurate and up-to-date information for their analyses and applications.

The NLCD 2019 and NLCD 2016 design is formulated to offer innovative, consistent, and robust methodologies for generating a multi-temporal land cover and land cover change database spanning from 2001 to 2019 at 2-3-year intervals. The development process involved extensive research, leading to the implementation of several key strategies for NLCD 2019, including the continued integration of impervious surface with all land cover products, a streamlined compositing process based on Landsat imagery and geospatial ancillary data sets, a comprehensive approach to training data development using multiple sources and decision-tree-based land cover classifications, a strategy for temporally, spectrally, and spatially integrated land cover change analysis, a hierarchical theme-based post-classification and integration protocol for generating land cover

and change products, a modeling method for continuous fields biophysical parameters, and the establishment of an automated scripted operational system for NLCD 2019 production.

NLCD 2011 provides, for the first time, the capability to assess wall-to-wall, spatially explicit, national land cover changes and trends across the U.S. from 2001 to 2011. As with two previous NLCD land cover products, NLCD 2011 keeps the same 16-class land cover classification scheme that has been applied consistently across the U.S. at a spatial resolution of 30 meters. NLCD 2011 is based primarily on a decision-tree classification of circa 2011 Landsat satellite data.

National Land Cover Database 2006 (NLCD 2006) is a 16-class land cover classification scheme that has been applied consistently across the conterminous U.S. at a spatial resolution of 30 meters. NLCD 2006 is based primarily on a decision-tree classification of circa 2006 Landsat satellite data. NLCD 2006 also quantifies land cover change between the years 2001 to 2006. The NLCD 2006 land cover change product was generated by comparing spectral characteristics of Landsat imagery between 2001 and 2006, on an individual path/row basis, using protocols to identify and label change based on the trajectory from NLCD 2001 products.

National Land Cover Database 2001 (NLCD 2001) is a 16-class (additional four classes in Alaska only) land cover classification scheme that has been applied consistently across all 50 states of the U.S. and Puerto Rico at a spatial resolution of 30 meters. NLCD 2001 is based primarily on a decision-tree classification of circa 2001 Landsat satellite data. NLCD 2001 improves on NLCD92 in that it is comprised of three different elements: land cover, percent developed impervious surface, and percent tree canopy density.

To understand how the urban landscape has changed across Louisiana, NLCDs from 2001, 2006, 2011, 2016, 2019. and 2021 were obtained. Pixel values that are classified as “Developed” (21, 22, 23, and 24) were used to define an urban location in Louisiana for each NLCD. Once the urban pixels were selected for each database, a cross-comparison was conducted using the raster calculator made available in ArcGIS. This method determines how the urban landscape has changed between the periods of 2001 to 2006, 2006 to 2011, 2011 to 2016, 2016 to 2019, and 2019 to 2021 for the state of Louisiana and its major cities (Shreveport, Monroe, Alexandria, Lake Charles, Lafayette, Houma, Baton Rouge, and New Orleans).

Developed	
21	**Developed, Open Space** - areas with a mixture of some constructed materials, but mostly vegetation in the form of lawn grasses. Impervious surfaces account for less than 20% of total cover. These areas most commonly include large-lot single-family housing units, parks, golf courses, and vegetation planted in developed settings for recreation, erosion control, or aesthetic purposes.
22	**Developed, Low Intensity** - areas with a mixture of constructed materials and vegetation. Impervious surfaces account for 20% to 49% percent of total cover. These areas most commonly include single-family housing units.
23	**Developed, Medium Intensity** - areas with a mixture of constructed materials and vegetation. Impervious surfaces account for 50% to 79% of the total cover. These areas most commonly include single-family housing units.
24	**Developed, High Intensity** - highly developed areas where people reside or work in high numbers. Examples include apartment complexes, row houses and commercial/ industrial. Impervious surfaces account for 80% to 100% of the total cover.

Vulnerable populations

Age demographics

Age demographic population estimations for young (<20 years old) and aging (>64 years old) populations were calculated at the parish level of each Louisiana parish for the year of 2050. Annual American Community Survey (ACS) 5-year estimates of the Age and Sex File (S0101) from 2012 to 2021 were obtained from U.S. Census Bureau American Fact Finder for each parish. The file consists of yearly population estimates (Pyear) for each parish from 2012 to 2021. These population estimates were used to calculate how the population changed in recent history until 2021 for each parish. The overall average rate (r) of vulnerable population change was calculated based of the nine annual population changes determined for each parish (Equation 1).

Average population vulnerable population change from 2012 to 2021:

$$r = \left(\frac{(P_{13} - P_{12})}{P_{12}} + \frac{(P_{14} - P_{13})}{P_{13}} + \frac{(P_{15} - P_{14})}{P_{14}} + \frac{(P_{16} - P_{15})}{P_{15}} + \cdots + \frac{(P_{20} - P_{19})}{P_{19}} + \frac{(P_{21} - P_{20})}{P_{20}}\right) / 9 \quad \text{(Equation 1)}$$

Positive rates of change indicate parishes that have experienced increases in vulnerable populations over the past nine years. Negative rates of change indicate parishes that have experienced overall average decreases in vulnerable populations over the past nine years.

Using the same growth rate model, the following rates of change of vulnerable populations were evaluated.

Disability demographics

Annual ACS 5-year estimates of Disability Characteristics (S1810) data were obtained from U.S. Census Bureau American Fact Finder for each parish from 2012 to 2021.

Poverty demographics

Annual ACS 5-year estimates of Poverty Status in the Past 12 Months (S1701) data were obtained from U.S. Census Bureau American Fact Finder for each parish from 2012 to **2021.**

Manufactured home estimates

Annual ACS 5-year estimates of Physical Housing Characteristics for Occupied Housing Units (S2504) data were obtained from U.S. Census Bureau American Fact Finder for each parish from 2012 to 2021.

The table below gives the parish level average annual growth rates for each identified vulnerable population. These values are summed by parish to provide an overarching indication of the direction of change for each parish across populations, where higher positive numbers indicate increased vulnerability, and higher negative numbers indicate

decreased vulnerability. Rates closer to zero indicate less change from the current populations. The change rates are also averaged for the parishes, showing that on average, across the state, change in demographic vulnerability is modest in a positive or negative direction. By contrast, many parishes show more exaggerated increases in vulnerable populations. The parishes with the highest sum of vulnerable population growth rates, indicating a greater likelihood of future increase in demographic vulnerability, are St. Bernard, Plaquemines, Ascension, St. Tammany, West Baton Rouge, and Richland parishes. It is noted that no parishes have a negative growth rate for aging populations, defined as older than 64 years old.

Table X: Average annual vulnerable population growth rates; positive values indicate increases in vulnerability while negative values indicate decreases in vulnerability.

Parish	Younger than 20	Older than 64	Population with disabilities	Population living in poverty	Population living in mobile Homes	Sum of vulnerable population growth rates
Acadia	-1%	2%	0%	2%	-2%	1%
Allen	-2%	0%	1%	0%	0%	-1%
Ascension	1%	5%	3%	0%	0%	9%
Assumption	-2%	3%	-2%	-2%	0%	-3%
Avoyelles	-1%	1%	1%	1%	0%	2%
Beauregard	0%	2%	2%	0%	1%	5%
Bienville	-2%	0%	-2%	0%	1%	-3%
Bossier	0%	3%	2%	4%	-2%	7%
Caddo	-1%	2%	1%	1%	-1%	2%
Calcasieu	1%	3%	-1%	1%	0%	4%
Caldwell	-1%	2%	-1%	1%	2%	3%
Cameron	-3%	1%	-3%	-2%	-3%	-10%
Catahoula	-3%	0%	-4%	1%	1%	-5%
Claiborne	-4%	0%	-3%	0%	2%	-5%
Concordia	-2%	1%	0%	0%	-4%	-5%
De Soto	0%	2%	2%	1%	0%	5%
East Baton Rouge	0%	3%	2%	0%	-1%	4%

East Carroll	-2%	2%	-1%	-2%	9%	6%
East Feliciana	-2%	3%	-3%	-5%	1%	-6%
Evangeline	-2%	1%	3%	2%	0%	4%
Franklin	-1%	1%	-5%	-1%	2%	-4%
Grant	-1%	2%	-2%	-1%	-2%	-4%
Iberia	-1%	2%	0%	1%	-1%	1%
Iberville	-2%	2%	0%	0%	0%	0%
Jackson	-2%	1%	-1%	0%	-2%	-4%
Jefferson	0%	3%	2%	1%	1%	7%
Jefferson Davis	0%	1%	-2%	0%	-1%	-2%
Lafayette	0%	4%	1%	1%	-1%	5%
Lafourche	-1%	2%	1%	1%	-1%	2%
LaSalle	0%	2%	-1%	6%	-1%	6%
Lincoln	0%	2%	1%	1%	2%	6%
Livingston	0%	4%	0%	-1%	-1%	2%
Madison	-2%	0%	2%	-3%	-5%	-8%
Morehouse	-1%	1%	-3%	1%	-2%	-4%
Natchitoches	-1%	2%	-2%	-1%	-1%	-3%
Orleans	0%	5%	1%	0%	-9%	-3%
Ouachita	0%	3%	2%	1%	-1%	5%
Plaquemines	0%	2%	3%	6%	1%	12%
Pointe Coupee	-2%	2%	4%	0%	0%	4%
Rapides	-1%	2%	-1%	-1%	3%	2%
Red River	-3%	1%	1%	-1%	0%	-2%
Richland	-1%	2%	1%	4%	2%	8%
Sabine	-1%	1%	-1%	0%	2%	1%
St. Bernard	3%	5%	6%	5%	-2%	17%
St. Charles	-1%	4%	0%	-2%	-2%	-1%
St. Helena	-2%	3%	3%	0%	2%	6%

St. James	-2%	2%	-1%	-3%	1%	-3%
St. John the Baptist	-2%	3%	-1%	-1%	0%	-1%
St. Landry	0%	2%	0%	0%	-1%	1%
St. Martin	-1%	3%	0%	0%	1%	3%
St. Mary	-2%	2%	-1%	-1%	-2%	-4%
St. Tammany	1%	5%	3%	2%	-2%	9%
Tangipahoa	1%	4%	3%	0%	-1%	7%
Tensas	-2%	2%	-2%	1%	-1%	-2%
Terrebonne	-1%	3%	0%	1%	-1%	2%
Union	-1%	2%	-2%	-1%	3%	1%
Vermilion	-1%	2%	2%	0%	-2%	1%
Vernon	-1%	2%	1%	3%	-2%	3%
Washington	-1%	2%	-1%	-1%	2%	1%
Webster	-2%	1%	-3%	1%	-2%	-5%
West						
Baton Rouge	1%	4%	1%	2%	1%	9%
West Carroll	-2%	0%	-1%	-1%	1%	-3%
West Feliciana	-1%	4%	-4%	1%	5%	5%
Winn	-2%	1%	-3%	-2%	-4%	-10%

Risk Assessment Approaches

The risk assessment calculates average annual losses in 2050 using an approach that considers the annual probability of occurrence and loss given that occurrence.

SHELDUS Loss Approach

For extreme heat, drought, extreme cold, hail, lightning, and tornado hazards, the planning team used the SHELDUS per capita property loss data to calculate losses at the census block level. This value is adjusted to 2021 dollars, but it is not population-adjusted. The team then normalized the SHELDUS average per capita property loss by the hazard intensity and population, to represent hazard loss properly as a function of hazard and population.

$$PL_{i,k,2050} = \frac{\overline{C_{J,k}} \sum_{i=1}^{i} P_{i,2020}}{\sum_{i=1}^{n} (H_{i,k} \times P_{i,2020})} \times H_{i,k} \times F_{k,2050} \times P_{i,2050}$$

where,

$PL_{i,k,2050}$ = projected annual property loss of census block i for hazard k in 2050
$\overline{C_{j,k}}$ = SHELDUS average per capita property loss (2021 dollars) of parish j for hazard k
$P_{i,2020}$ = population of census block i in 2020
$H_{i,k}$ = historical hazard intensity of census block i for hazard k
$F_{k,2050}$ = future hazard multification factor for hazard k in 2050
$P_{i,2050}$ = projected population in census block i in 2050

Crop Loss

The planning team used the SHELDUS average annual crop loss data, which is already adjusted to 2021 dollars, to calculate the losses by census block. The team did not consider population growth in the annual crop loss of each census block.

.

$$CL_{j,k,2050} = \frac{\bar{C}_{j,k}}{\sum_{i=1}^{n} (H_{i,k} \times CLC_{i,2016})} \times H_{i,k} \times F_{k,2050} \times CIC_{2050} \times CLC_{i,2050}$$

$$CIC_{2050} = CD_{2050} \times CL_{2050}$$

$$CD_{2050} = 1 + (C_{World} \times P_{World,2050} + C_{US} \times P_{US,2050})$$

where

$CL_{2050,i}$ = projected annual crop loss of census block i in 2050
$\bar{C}_{j,k}$ = SHELDUS historical average annual crop loss (2021 dollars) of parish j for hazard k
$CLC_{k,2021}$= crop land cover area in census block i in 2021
F_i= future hazard multification factor for census block i in 2050
$H_{i,k}$ = historical hazard intensity of census block i for hazard k
$F_{k,2050}$ = future hazard multification factor for hazard k in 2050
CIC_{2050} = future cropping intensity and technological development coefficien in 2050
$CLC_{i,2050}$ = projected crop land cover area in census block i in 2050
CD_{2050} = consumer demand coefficient of Louisiana crops in 2050
CL_{2050}= the projected crop land cover coefficient in 2050
C_{World}= percent of Louisiana's crop consumed by the rest of the world
$P_{World,2050}$ = percent of world population increase by 2050
C_{US} = percent of Louisiana's crop consumed within United States
$P_{US,2050}$ = percent of U. S. population increase by 2050

Alternative Loss Approaches

For wildfire, sinkholes, and expansive soil, we developed customized loss estimation approaches based on consultation with state agencies and members of the SHMPC. For wind and flood, loss estimation used the data from FEMA's Hazus-MH model and USACE's National Structure Inventory (NSI). The methods for alternative loss approaches are described in the following sections.

State Asset Loss Approach

All state buildings are vulnerable to hazards. At the state level, historic hazard losses for state buildings and detailed building stock information are lacking. These data limitations preclude utilization of either of the previously defined loss approaches. Therefore, because of this data deficiency and in consultation with the Louisiana Department of Insurance, the planning team derived a methodology to estimate average annual state asset losses. The methodology assumes that average annual losses for state buildings would echo historic/modeled losses for other occupancies, considering that the state building inventory is representative of the total building inventory in Louisiana.

Utilizing building-level data from the Louisiana Office of Risk Management, 8,783 state buildings were included in the loss assessment, considering a total building and contents replacement value of approximately $15.2 billion. The following table details the buildings considered in each parish, along with the replacement value of state buildings and the total building value within each parish. State asset losses were calculated using the ratio of state property value to total property value (building + contents) and multiplied by the loss assessment results for each individual hazard. State asset losses are included in the total loss results and also reported separately.

Parish	State Building Count	State Property Value ($)	Total Property Value ($)
Acadia	126	$183,189,471	$12,761,905,085
Allen	56	$68,193,547	$4,017,410,850
Ascension	27	$67,862,280	$35,674,794,234
Assumption	5	$2,320,851	$3,715,586,559
Avoyelles	156	$146,390,032	$7,311,449,264
Beauregard	107	$65,518,466	$6,698,350,732
Bienville	12	$4,898,386	$2,830,101,125
Bossier	148	$233,285,613	$23,065,813,208

Caddo	194	$847,673,180	$52,556,450,950
Calcasieu	231	$747,741,258	$47,636,460,693
Caldwell	34	$15,340,851	$1,785,678,747
Cameron	31	$29,618,272	$1,421,615,071
Catahoula	16	$3,988,782	$1,686,489,971
Claiborne	167	$86,305,383	$3,083,461,617
Concordia	30	$28,141,054	$3,538,510,424
DeSoto	24	$13,646,343	$4,430,351,606
East Baton Rouge	783	$965,758,591	$122,348,231,945
East Carroll	27	$11,186,373	$1,463,463,101
East Feliciana	265	$346,102,492	$6,405,477,364
Evangeline	81	$32,005,695	$5,414,736,987
Franklin	63	$33,489,343	$3,432,021,380
Grant	69	$23,576,395	$3,063,977,392
Iberia	131	$171,485,060	$12,732,962,273
Iberville	321	$381,631,771	$5,977,485,681
Jackson	60	$17,690,820	$3,352,879,006
Jefferson	156	$407,866,828	$74,820,010,581
Jefferson Davis	30	$42,799,794	$5,946,871,734
Lafayette	276	$1,579,944,999	$55,420,596,002
Lafourche	139	$604,069,060	$15,491,623,352
LaSalle	41	$14,124,912	$2,402,384,690
Lincoln	343	$1,584,185,490	$8,249,776,981
Livingston	68	$49,346,930	$26,435,675,788
Madison	66	$48,662,532	$1,568,864,843
Morehouse	45	$15,086,595	$5,566,498,859
Natchitoches	142	$483,728,847	$7,737,165,719
Orleans	563	$1,085,772,704	$73,039,836,872
Ouachita	278	$901,720,320	$35,572,945,453

Plaquemines	20	$6,974,739	$6,301,745,322
Pointe Coupee	20	$9,750,411	$5,416,174,616
Rapides	982	$913,754,399	$27,654,248,737
Red River	9	$4,791,058	$1,706,662,982
Richland	68	$29,064,451	$4,152,157,065
Sabine	190	$49,472,698	$5,616,258,528
St. Bernard	47	$122,114,695	$7,269,805,346
St. Charles	5	$2,137,969	$10,258,854,277
St. Helena	14	$17,158,995	$1,688,091,274
St. James	3	$794,614	$6,310,538,269
St. John the Baptist	32	$95,268,663	$8,836,443,087
St. Landry	42	$59,752,471	$17,074,198,676
St. Martin	75	$71,406,746	$11,234,018,710
St. Mary	36	$56,441,020	$16,476,516,936
St. Tammany	145	$137,197,087	$45,050,334,430
Tangipahoa	274	$1,069,782,861	$23,861,838,450
Tensas	48	$12,968,024	$1,586,902,328
Terrebonne	45	$140,550,909	$27,417,613,412
Union	50	$11,994,968	$4,684,704,278
Vermilion	75	$43,869,321	$7,510,038,951
Vernon	68	$40,369,279	$7,464,498,315
Washington	186	$122,513,647	$8,113,186,898
Webster	353	$207,407,868	$12,299,311,315
West Baton Rouge	16	$14,876,223	$6,255,435,681
West Carroll	24	$9,925,633	$1,809,568,702
West Feliciana	564	$508,026,607	$2,805,960,545
Winn	81	$91,009,729	$2,626,678,901
Total	8,783	$15,193,724,405	$970,139,702,171

Risk Assessment Results

Property Loss Results

The following parish-level property losses were determined for each hazard. All losses represent average annual losses, and the parish total reflects the summation of these values to portray the relative risk for Louisiana parishes.

Parish	Wildfire Property Loss	Extreme Cold Property Loss	Wind Property Loss	Hail Property Loss	Lightning Property Loss
Acadia	$43,081	$109,225	$18,976,095	$2,279	$9,263
Allen	$430,960	$133,528	$2,283,424	$1,214	$11,188
Ascension	$1,044,837	$829,971	$71,081,674	$35,304	$111,734
Assumption	$678	$93,815	$8,465,731	$4,164	$17,346
Avoyelles	$76,552	$135,698	$1,946,783	$15,922	$34,921
Beauregard	$932,945	$260,788	$3,713,809	$5,473	$24,375
Bienville	$96,067	$72,618	$54,794	$949	$12,842
Bossier	$1,049,712	$361,084	$403,395	$474,036	$553,536
Caddo	$1,447,672	$2,302,449	$484,708	$193,647	$34,794
Calcasieu	$1,891,692	$216,945	$68,915,361	$804,736	$42,227
Caldwell	$54,886	$94,320	$97,434	$1,575	$10,051
Cameron	$18,267	$32,204	$2,852,792	$327	$3,349
Catahoula	$22,011	$65,380	$113,551	$10,168	$6,075
Claiborne	$115,159	$75,642	$49,288	$1,211	$3,277
Concordia	$6,360	$89,947	$370,669	$5,361	$8,342
DeSoto	$113,314	$149,631	$154,410	$2,808	$2,179
East Baton Rouge	$1,815,265	$198,391	$87,071,815	$83,656	$258,652
East Carroll	$6,023	$62,274	$32,686	$4,182	$4,529
East Feliciana	$191,027	$82,200	$1,439,261	$3,447	$468

Evangeline	$178,868	$90,370	$3,224,871	$1,968	$11,730
Franklin	$23,195	$95,749	$196,802	$24,052	$14,291
Grant	$216,290	$207,188	$509,932	$2,773	$27,761
Iberia	$1,313	$113,998	$27,717,448	$1,221	$28,258
Iberville	$9,256	$127,525	$6,532,949	$3,412	$3,287
Jackson	$121,727	$93,024	$121,221	$1,401	$6,161
Jefferson	$312,244	$158,323	$136,541,928	$1,276,719	$22,317
Jefferson Davis	$86,092	$151,216	$11,506,461	$2,117	$26,809
Lafayette	$48,647	$442,289	$102,021,247	$3,690	$186,885
Lafourche	$1,451	$173,436	$66,709,800	$7,493	$7,176
LaSalle	$136,552	$118,546	$248,638	$3,374	$12,713
Lincoln	$354,867	$219,949	$192,029	$10,781	$17,501
Livingston	$3,021,288	$886,024	$44,095,016	$38,668	$1,703,676
Madison	$2,774	$52,335	$64,720	$12,305	$381
Morehouse	$88,787	$89,594	$80,092	$47,665	$1,026
Natchitoches	$275,526	$99,346	$435,297	$7,551	$15,633
Orleans	$701,272	$59,511	$126,031,732	$6,017	$13,592
Ouachita	$780,221	$198,896	$788,678	$190,017	$21,373
Plaquemines	$14,442	$77,231	$18,477,371	$4,535	$1,318
Pointe Coupee	$10,316	$116,390	$2,907,389	$7,897	$1,650
Rapides	$1,577,914	$168,614	$3,378,896	$3,636	$18,292
Red River	$38,831	$70,220	$34,325	$986	$1,176
Richland	$41,717	$103,569	$129,494	$15,254	$5,683
Sabine	$222,821	$131,239	$519,470	$5,421	$12,223
St. Bernard	$112,732	$196,535	$28,042,826	$9,760	$1,580
St. Charles	$12,185	$234,538	$18,430,989	$12,670	$17,470
St. Helena	$204,755	$114,829	$1,024,743	$4,632	$858
St. James	$16,265	$93,138	$7,443,881	$3,743	$34,373
St. John the Baptist	$38,878	$183,549	$11,439,528	$8,403	$858

St. Landry	$96,645	$92,149	$13,299,187	$842	$10,277
St. Martin	$7,308	$179,286	$15,924,562	$1,761	$145,966
St. Mary	$353	$78,509	$34,617,551	$3,532	$14,841
St. Tammany	$6,055,785	$907,727	$116,499,172	$572,683	$86,438
Tangipahoa	$4,081,624	$320,804	$22,417,890	$22,591	$98,181
Tensas	$963	$26,941	$78,852	$7,025	$2,236
Terrebonne	$621	$162,086	$105,325,259	$6,387	$26,715
Union	$114,385	$126,315	$117,431	$2,391	$4,642
Vermilion	$2,321	$149,918	$29,576,452	$11,127	$19,897
Vernon	$648,276	$162,281	$1,475,941	$5,736	$14,928
Washington	$704,415	$104,081	$7,827,702	$4,773	$8,762
Webster	$445,566	$91,907	$112,333	$3,333	$10,720
West Baton Rouge	$24,619	$342,510	$5,339,153	$11,017	$2,159
West Carroll	$15,730	$82,688	$39,927	$7,851	$500
West Feliciana	$17,333	$127,212	$980,090	$1,254	$2,060
Winn	$100,861	$62,355	$102,624	$2,047	$6,673
Total Loss	$30,324,536	$13,250,045	$1,241,089,577	$4,032,967	$3,820,196

Crop Loss Results

The following parish-level crop losses were determined for each hazard. All losses represent average annual losses, with the exception of flood hazards.

Parish	Extreme Heat Crop Loss	Drought Crop Loss	Extreme Cold Crop Loss	Hail Crop Loss	Lightning Crop Loss	Tornado Crop Loss	Parish Average Annual Crop Loss
Acadia	$17,137	$2,045,651	$16,082	$910	$55	$105,949	$2,185,783
Allen	$15,914	$1,091,979	$14,880	$129	$51	$219	$1,123,172
Ascension	$14,810	$318,261	$37,322	$117	$48	$13	$370,571
Assumption	$17,229	$2,384,705	$42,819	$541	$55	$83	$2,445,432
Avoyelles	$17,126	$3,752,972	$18,415	$137	$96	$209	$3,788,954
Beauregard	$14,802	$945,399	$13,902	$324	$351	-	$974,778
Bienville	$15,258	$77,426	$17,583	$132	$50	$14	$110,462
Bossier	$14,569	$161,131	$16,801	$117	$48	$121	$192,786
Caddo	$15,099	$8,385,258	$17,378	$1,552	$49	$181	$8,419,517
Calcasieu	$16,202	$2,102,749	$15,089	$129	$52	$5	$2,134,226
Caldwell	$17,671	$89,747	$20,335	$186	$60	-	$127,999
Cameron	$15,914	$335,991	$14,983	$130	$562	-	$367,580
Catahoula	$16,997	$197,421	$18,294	$18,430	$55	$28,665	$279,861
Claiborne	$15,616	$79,240	$17,996	$127	$51	$261	$113,292
Concordia	$17,166	$218,617	$18,414	$16,297	$511	$32,257	$303,261
DeSoto	$12,015	$132,851	$13,913	$397	$40	-	$159,215
East Baton Rouge	$14,348	$517,025	$35,718	$393	$46	$13	$567,544
East Carroll	$17,315	$335,036	$19,965	$17,543	$109	$21,699	$411,667
East Feliciana	$12,976	$765,251	$31,636	$109	$41	$284	$810,297
Evangeline	$16,869	$1,289,329	$17,315	$658	$54	$15	$1,324,240
Franklin	$17,520	$265,814	$20,231	$35,638	$58	$7	$339,268
Grant	$15,623	$79,881	$16,864	$144	$51	$119	$112,682
Iberia	$16,655	$1,035,531	$15,632	$134	$54	$15	$1,068,020
Iberville	$16,550	$481,546	$41,287	$132	$53	$15	$539,584
Jackson	$14,626	$74,453	$16,773	$153	$48	-	$106,052
Jefferson	$13,278	$279,267	$34,379	$230	$44	$29	$327,227
Jefferson Davis	$17,045	$2,199,231	$15,970	$137	$55	$22	$2,232,459

Lafayette	$15,722	$1,853,637	$14,716	$134	$50	$25	$1,884,284
Lafourche	$16,234	$549,846	$40,750	$130	$51	$14	$607,026
LaSalle	$16,293	$82,730	$17,472	$321	$52	-	$116,869
Lincoln	$15,035	$76,325	$17,358	$178	$49	$84	$109,029
Livingston	$13,688	$811,498	$33,896	$107	$44	$586	$859,818
Madison	$17,048	$269,745	$20,010	$28,842	$56	$27,075	$362,776
Morehouse	$17,138	$297,373	$19,656	$611	$56	$24,251	$359,085
Natchitoches	$15,786	$80,098	$16,926	$182	$51	$1,876	$114,919
Orleans	$16,207	$329,739	$40,249	$277	$52	$15	$386,539
Ouachita	$16,619	$84,514	$19,125	$967	$55	$36	$121,316
Plaquemines	$10,545	$205,312	$25,773	$244	$33	$10	$241,916
Pointe Coupee	$17,195	$929,586	$41,210	$138	$55	$15	$988,199
Rapides	$16,735	$1,825,785	$17,967	$2,198	$54	$5,826	$1,868,566
Red River	$15,039	$76,369	$17,323	$130	$50	-	$108,911
Richland	$17,253	$297,442	$20,292	$5,094	$57	$32	$340,169
Sabine	$15,580	$171,978	$16,706	$2,223	$50	$2,232	$208,769
St. Bernard	$14,174	$294,783	$36,184	$246	$47	$13	$345,448
St. Charles	$15,664	$345,926	$39,368	$263	$51	$14	$401,286
St. Helena	$12,856	$1,161,536	$31,824	$104	$41	$283	$1,206,644
St. James	$19,916	$806,192	$40,355	$131	$52	$15	$866,661
St. John the Baptist	$16,230	$329,065	$40,302	$131	$52	$44,177	$429,957
St. Landry	$16,817	$3,485,047	$15,743	$578	$94	$103,768	$3,622,047
St. Martin	$16,750	$1,157,057	$15,731	$134	$54	$15	$1,189,742
St. Mary	$16,991	$1,255,931	$15,957	$137	$55	$15	$1,289,085
St. Tammany	$13,926	$285,219	$35,158	$113	$45	$13	$334,474
Tangipahoa	$13,475	$273,514	$33,813	$108	$43	$10,910	$331,863
Tensas	$17,301	$234,133	$19,955	$31,068	$57	$3,067	$305,582
Terrebonne	$14,392	$436,445	$36,296	$149	$46	$13	$487,341
Union	$15,317	$77,822	$17,682	$398	$74	$3	$111,296
Vermilion	$16,054	$4,095,274	$15,088	$142	$51	$26	$4,126,635
Vernon	$16,182	$6,917	$17,379	$175	$52	$5,834	$46,540
Washington	$13,214	$863,789	$32,972	$107	$48	$3,932	$914,062
Webster	$14,640	$74,322	$16,857	$142	$48	$2	$106,011

West Baton Rouge	$16,783	$401,571	$41,432	$134	$54	$15	$459,988
West Carroll	$17,077	$296,049	$19,679	$2,970	$134	$332	$336,241
West Feliciana	$13,891	$426,917	$33,249	$110	$44	$12	$474,223
Winn	$12,537	$63,494	$13,406	$281	$41	$361	$90,120
Total Loss	**$1,002,631**	**$53,954,740**	**$1,527,834**	**$174,325**	**$4,745**	**$425,091**	**$57,089,365**

Total Loss Results

The following parish level total (property and crop) losses were determined for each hazard. All losses represent average annual losses, and the parish total reflects the summation of these values, to portray the relative risk for Louisiana parishes.

Lightning Loss	Tornado Loss	Flood Loss	Earthquake Loss	Sinkhole Loss	Expansive Soil Loss	Parish Average Annual Loss
$9,318	$1,036,581	$18,425,191	$80,874	$171,242	$674,209	$41,527,000
$11,239	$23,538	$2,671,918	$26,709	-	$156,984	$6,835,707
$111,782	$464,886	$52,340,977	$527,442	$3,242	$7,053,207	$133,336,391
$17,401	$51,615	$19,702,188	$20,474	$2,155	$573,336	$31,356,376
$35,016	$155,369	$28,150,312	$85,809	$-	$108,340	$34,412,643
$24,726	$269,029	$2,126,313	$54,800	$374	$154,403	$8,462,287
$12,892	$157,157	$8,749,796	$45,120	$4,312	$28,391	$9,287,374
$553,584	$9,690,243	$32,912,641	$693,651	-	$489,890	$46,127,201
$34,843	$1,070,304	$16,784,058	$933,517	-	$585,454	$31,322,422
$42,279	$552,635	$169,161,544	$280,885	$177,929	$4,028,018	$247,925,307
$10,112	$81,796	$2,264,200	$32,263	$61	$183,049	$2,915,372
$3,910	$25,496	$139,940,134	$2,724	$8,723	$88,293	$143,337,164
$6,130	$84,293	$5,148,022	$28,071	$1,320	$72,592	$5,774,607
$3,328	$176,354	$10,059,884	$55,921	$112	$34,502	$10,628,460
$8,853	$94,398	$1,472,192	$64,352	-	$172,104	$2,490,377
$2,219	$547,968	$1,394,269	$62,516	-	$72,860	$2,596,654
$258,698	$322,084	$137,866,362	$1,248,538	-	$10,319,714	$238,503,472
$4,638	$78,564	$3,878,129	$92,162	-	$30,131	$4,486,486
$509	$15,314	$1,081,581	$44,754	-	$59,593	$3,682,905
$11,784	$121,108	$3,601,291	$42,786	$1,314	$96,134	$8,651,877
$14,349	$34,865	$1,708,592	$124,207	$3,208	$128,531	$2,568,548
$27,811	$30,166	$1,523,423	$51,665	$-	$220,571	$2,850,668
$28,311	$147,671	$24,461,415	$64,541	$3,429	$907,874	$54,450,631
$3,341	$26,597	$3,067,641	$40,872	$18,741	$643,170	$10,972,147
$6,210	$61,560	$12,950,426	$78,972	$347	$157,942	$13,619,862

Jefferson	$13,278	$279,267	$312,244	$192,702	$136,541,928	$1,276,949
Jefferson Davis	$17,045	$2,199,231	$86,092	$167,185	$11,506,461	$2,254
Lafayette	$15,722	$1,853,637	$48,647	$457,005	$102,021,247	$3,824
Lafourche	$16,234	$549,846	$1,451	$214,186	$66,709,800	$7,623
LaSalle	$16,293	$82,730	$136,552	$136,018	$248,638	$3,695
Lincoln	$15,035	$76,325	$354,867	$237,306	$192,029	$10,960
Livingston	$13,688	$811,498	$3,021,288	$919,920	$44,095,016	$38,774
Madison	$17,048	$269,745	$2,774	$72,345	$64,720	$41,147
Morehouse	$17,138	$297,373	$88,787	$109,250	$80,092	$48,275
Natchitoches	$15,786	$80,098	$275,526	$116,272	$435,297	$7,733
Orleans	$16,207	$329,739	$701,272	$99,760	$126,031,732	$6,294
Ouachita	$16,619	$84,514	$780,221	$218,020	$788,678	$190,984
Plaquemines	$10,545	$205,312	$14,442	$103,004	$18,477,371	$4,779
Pointe Coupee	$17,195	$929,586	$10,316	$157,600	$2,907,389	$8,035
Rapides	$16,735	$1,825,785	$1,577,914	$186,581	$3,378,896	$5,834
Red River	$15,039	$76,369	$38,831	$87,543	$34,325	$1,116
Richland	$17,253	$297,442	$41,717	$123,860	$129,494	$20,348
Sabine	$15,580	$171,978	$222,821	$147,945	$519,470	$7,644
St. Bernard	$14,174	$294,783	$112,732	$232,720	$28,042,826	$10,006
St. Charles	$15,664	$345,926	$12,185	$273,906	$18,430,989	$12,933
St. Helena	$12,856	$1,161,536	$204,755	$146,652	$1,024,743	$4,736
St. James	$19,916	$806,192	$16,265	$133,494	$7,443,881	$3,874
St. John the Baptist	$16,230	$329,065	$38,878	$223,851	$11,439,528	$8,533
St. Landry	$16,817	$3,485,047	$96,645	$107,892	$13,299,187	$1,420
St. Martin	$16,750	$1,157,057	$7,308	$195,017	$15,924,562	$1,895
St. Mary	$16,991	$1,255,931	$353	$94,466	$34,617,551	$3,669
St. Tammany	$13,926	$285,219	$6,055,785	$942,884	$116,499,172	$572,796
Tangipahoa	$13,475	$273,514	$4,081,624	$354,617	$22,417,890	$22,700
Tensas	$17,301	$234,133	$963	$46,896	$78,852	$38,093
Terrebonne	$14,392	$436,445	$621	$198,382	$105,325,259	$6,536
Union	$15,317	$77,822	$114,385	$143,998	$117,431	$2,789

Vermilion	$16,054	$4,095,274	$2,321	$165,006	$29,576,452	$11,269
Vernon	$16,182	$6,917	$648,276	$179,660	$1,475,941	$5,912
Washington	$13,214	$863,789	$704,415	$137,053	$7,827,702	$4,880
Webster	$14,640	$74,322	$445,566	$108,764	$112,333	$3,475
West Baton Rouge	$16,783	$401,571	$24,619	$383,943	$5,339,153	$11,151
West Carroll	$17,077	$296,049	$15,730	$102,367	$39,927	$10,821
West Feliciana	$13,891	$426,917	$17,333	$160,461	$980,090	$1,363
Winn	$12,537	$63,494	$100,861	$75,761	$102,624	$2,328
Total Loss	**$1,002,631**	**$53,954,740**	**$30,324,536**	**$14,777,880**	**$1,241,089,577**	**$4,207,292**

State Asset Loss Results

The following parish-level state asset losses were determined for each hazard. All losses represent average annual losses, and the parish total reflects the summation of these values, to portray the relative risk for Louisiana parishes.

Tornado Property Loss	Flood Property Loss	Earthquake Property Loss	Sinkhole Property Loss	Expansive Soil Property Loss	State Property Average Annual Loss
$13,359	$264,483	$1,161	$2,458	$9,678	$564,720
$396	$45,354	$453	-	$2,665	$96,967
$884	$99,565	$1,003	$6	$13,417	$252,934
$32	$12,306	$13	$1	$358	$18,059
$3,107	$563,626	$1,718	-	$2,169	$613,148
$2,631	$20,798	$536	$4	$1,510	$73,237
$272	$15,144	$78	$7	$49	$15,884
$98,005	$332,876	$7,016	-	$4,955	$464,577
$17,260	$270,707	$15,057	-	$9,443	$369,397
$8,675	$2,655,299	$4,409	$2,793	$63,227	$3,858,140
$703	$19,452	$277	$1	$1,573	$23,946
$531	$2,915,547	$57	$182	$1,840	$2,978,663
$132	$12,176	$66	$3	$172	$12,996
$4,929	$281,574	$1,565	$3	$966	$294,317
$494	$11,708	$512	-	$1,369	$17,394

$1,688	$4,295	$193	-	$224	$7,508
$2,542	$1,088,251	$9,855	-	$81,459	$1,878,153
$435	$29,644	$704	-	$230	$31,147
$812	$58,440	$2,418	-	$3,220	$155,214
$716	$21,287	$253	$8	$568	$43,313
$340	$16,672	$1,212	$31	$1,254	$21,753
$231	$11,722	$398	-	$1,697	$21,068
$1,989	$329,442	$869	$46	$12,227	$718,947
$1,697	$195,853	$2,609	$1,196	$41,063	$666,066
$325	$68,330	$417	$2	$833	$71,303
$2,055	$1,137,207	$2,624	$87	$65,823	$1,959,151
$2,885	$107,191	$245	$158	$4,777	$199,738
$31,017	$9,195,997	$15,628	$293	$144,007	$12,299,191
$8,429	$4,371,223	$4,097	$546	$111,122	$7,099,945
$1,755	$59,863	$287	-	$623	$65,298
$236,995	$7,413,574	$65,294	$10	$68,790	$7,872,057
$547	$372,036	$798	-	$6,105	$471,545
$13,283	$25,625	$1,800	$38	$1,611	$44,668
$171	$2,984	$701	-	$162	$4,149
$13,398	$304,295	$8,425	$68	$27,019	$396,882
$2,209	$1,152,419	$8,235	-	$188,566	$3,228,318
$133,092	$537,196	$39,211	-	$43,641	$764,099
$25	$56,786	$34	$59	$651	$78,079
$100	$7,885	$78	-	$313	$13,777
$21,506	$3,663,565	$12,152	$1	$25,151	$3,880,300
$41	$14,477	$63	-	$79	$15,006
$343	$16,467	$1,231	-	$1,039	$19,919
$532	$176,950	$366	-	$748	$186,080
$594	$1,126,480	$1,365	$4	$47,611	$1,651,123
$7	$30,104	$13	$3	$505	$34,518
$296	$7,799	$179	-	$687	$22,503
$2	$1,775	$4	$2	$115	$2,850
$7,347	$574,643	$597	-	$16,878	$724,699

St. Landry	$338	$322	$46,542	$3	$36
St. Martin	$46	$1,140	$101,221	$11	$928
St. Mary	$1	$269	$118,584	$12	$51
St. Tammany	$18,442	$2,764	$354,789	$1,744	$263
Tangipahoa	$182,989	$14,382	$1,005,047	$1,013	$4,402
Tensas	$8	$220	$644	$57	$18
Terrebonne	$3	$831	$539,929	$33	$137
Union	$293	$323	$301	$6	$12
Vermilion	$14	$876	$172,769	$65	$116
Vernon	$3,506	$878	$7,982	$31	$81
Washington	$10,637	$1,572	$118,203	$72	$132
Webster	$7,514	$1,550	$1,894	$56	$181
West Baton Rouge	$59	$815	$12,697	$26	$5
West Carroll	$86	$454	$219	$43	$3
West Feliciana	$3,138	$23,032	$177,448	$227	$373
Winn	$3,495	$2,160	$3,556	$71	$231
Total	**$533,438**	**$225,656**	**$15,062,040**	**$42,060**	**$33,865**

Historic Properties Hazard Exposure

Because building and contents values are not available for many historic sites, hazard parameters were extracted for each of the evaluated historic properties, which can help inform risk for these properties.

700 Year Peak Gust Wind Speed (mph)	Hail Days per Year	Flashes/sq. mile/year	Tornado Days per Year	Soil Clay Content of High Swelling Potentiality (%)	Distance to the Nearest High Hazard Potential Dam (miles)	Distance to the Nearest Sinkhole (miles)	Flood Zone
105	2	12	1	<40	1.5	10.4	X
138	2	22	2	>40	64.4	9.8	X
138	2	22	2	>40	64.1	10.1	X
135	1	18	2	>40	50.5	3.5	A
105	2	12	1	<40	1.5	10.4	X
130	0	20	1	<40	35.4	5.5	X
160	0	13	1	<40	103.7	4.7	A
142	1	17	1	<40	51.0	17.6	VE
148	0	19	0	<40	70.0	6.3	VE
139	2	23	2	<40	64.3	9.4	X
105	3	12	1	<40	18.4	24.0	X
139	2	23	2	>40	64.7	9.1	X
139	2	22	2	>40	64.5	9.7	X
105	2	12	1	<40	1.5	10.4	X
105	2	13	1	<40	10.1	20.7	X
119	2	22	2	<40	5.0	7.2	X
139	2	22	2	>40	64.5	9.8	X
120	2	21	2	<40	3.3	7.8	X
139	2	22	2	>40	64.4	9.9	X
109	1	13	1	<40	19.6	14.6	X
105	2	13	1	<40	12.4	15.0	X
105	2	12	1	<40	1.4	10.5	X
131	0	18	1	<40	31.4	2.6	X

113	1	16	1	<40	6.5	20.8	X
105	2	12	1	<40	1.4	10.5	X
119	2	21	2	<40	4.4	7.4	X
119	2	21	2	<40	4.6	7.1	X
139	2	22	2	>40	64.6	9.9	X
139	2	22	2	>40	64.5	9.9	X
135	1	18	2	>40	49.2	2.9	A
130	0	18	1	<40	29.4	4.9	X
114	1	17	1	<40	12.9	14.8	X
105	2	11	1	<40	10.3	17.5	X
139	2	22	2	>40	64.4	9.8	X
105	2	12	1	<40	1.5	10.4	X
104	3	12	1	<40	19.0	13.4	X
144	0	11	1	<40	65.1	13.6	AE
130	0	20	1	<40	36.1	7.7	X
110	1	14	1	<40	9.5	16.4	X
138	2	22	2	>40	64.4	9.8	X
139	2	22	2	>40	64.4	9.7	X
139	2	22	2	<40	64.0	9.6	X
119	2	21	2	<40	4.6	7.0	AE

Historic Properties Hazard Exposure

Because building and contents values are not available for many historic sites, hazard parameters were extracted for each of the evaluated historic properties, which can help inform risk for these properties.

Hail Days per Year	Flashes/sq. mile/year	Tornado Days per Year	Soil Clay Content of High Swelling Potentiality (%)	Distance to the Nearest High Hazard Potential Dam (miles)	Distance to the Nearest Sinkhole (miles)	Flood Zone
2	12	1	<40	1.5	10.4	X
2	22	2	>40	64.4	9.8	X
2	22	2	>40	64.1	10.1	X
1	18	2	>40	50.5	3.5	A
2	12	1	<40	1.5	10.4	X
0	20	1	<40	35.4	5.5	X
0	13	1	<40	103.7	4.7	A
1	17	1	<40	51.0	17.6	VE
0	19	0	<40	70.0	6.3	VE
2	23	2	<40	64.3	9.4	X
3	12	1	<40	18.4	24.0	X
2	23	2	>40	64.7	9.1	X
2	22	2	>40	64.5	9.7	X
2	12	1	<40	1.5	10.4	X
2	13	1	<40	10.1	20.7	X
2	22	2	<40	5.0	7.2	X
2	22	2	>40	64.5	9.8	X
2	21	2	<40	3.3	7.8	X
2	22	2	>40	64.4	9.9	X
1	13	1	<40	19.6	14.6	X
2	13	1	<40	12.4	15.0	X

2	12	1	<40	1.4	10.5	X
0	18	1	<40	31.4	2.6	X
1	16	1	<40	6.5	20.8	X
2	12	1	<40	1.4	10.5	X
2	21	2	<40	4.4	7.4	X
2	21	2	<40	4.6	7.1	X
2	22	2	>40	64.6	9.9	X
2	22	2	>40	64.5	9.9	X
1	18	2	>40	49.2	2.9	A
0	18	1	<40	29.4	4.9	X
1	17	1	<40	12.9	14.8	X
2	11	1	<40	10.3	17.5	X
2	22	2	>40	64.4	9.8	X
2	12	1	<40	1.5	10.4	X
3	12	1	<40	19.0	13.4	X
0	11	1	<40	65.1	13.6	AE
0	20	1	<40	36.1	7.7	X
1	14	1	<40	9.5	16.4	X
2	22	2	>40	64.4	9.8	X
2	22	2	>40	64.4	9.7	X
2	22	2	<40	64.0	9.6	X
2	21	2	<40	4.6	7.0	AE

Changes in Future Hazard Conditions

Billion-dollar weather disasters, already at a relatively high frequency of approximately 2 per year for Louisiana (Figure X.Xa, which appears as Figure 22.3 in the recently available Fifth National Climate Assessment (NCA5; Jay et al., 2023; https://www.globalchange.gov/reports/fifth-national-climate-assessment-overview), have been exacerbated by several recent hurricane strikes (Figure X.Xb; Jay et al., 2023). To project changes in future conditions, NCA5 utilizes output from the Intergovernmental Panel for Climate Change (IPCC) reports, with specialized focus on each U.S. region. While useful, it is noteworthy that Louisiana appears on the southwestern edge of the Southeast U.S. region, both in NCA5 (Figure X.X) and in the IPCC reports (Figure X.Y). Thus, "bulk" projections of climatic changes for the U.S. Southeast may not always best represent the case of Louisiana. Furthermore, textual information in the NCA5 chapters was unavailable at this writing; only the figures and "Key Points" from the regional chapters (including Chapter 22 entitled "Southeast") were available. A key theme emphasized throughout NCA5 is that the risks resulting from current hazards are not distributed equitably, with health, economic, and social inequalities widened and felt disproportionately among those from underserved communities. The following sections describe the rationale behind our projections of changes in future hazard conditions and explain our specialized risk assessment approaches for hazards that did not use the SHELDUS loss methodology.

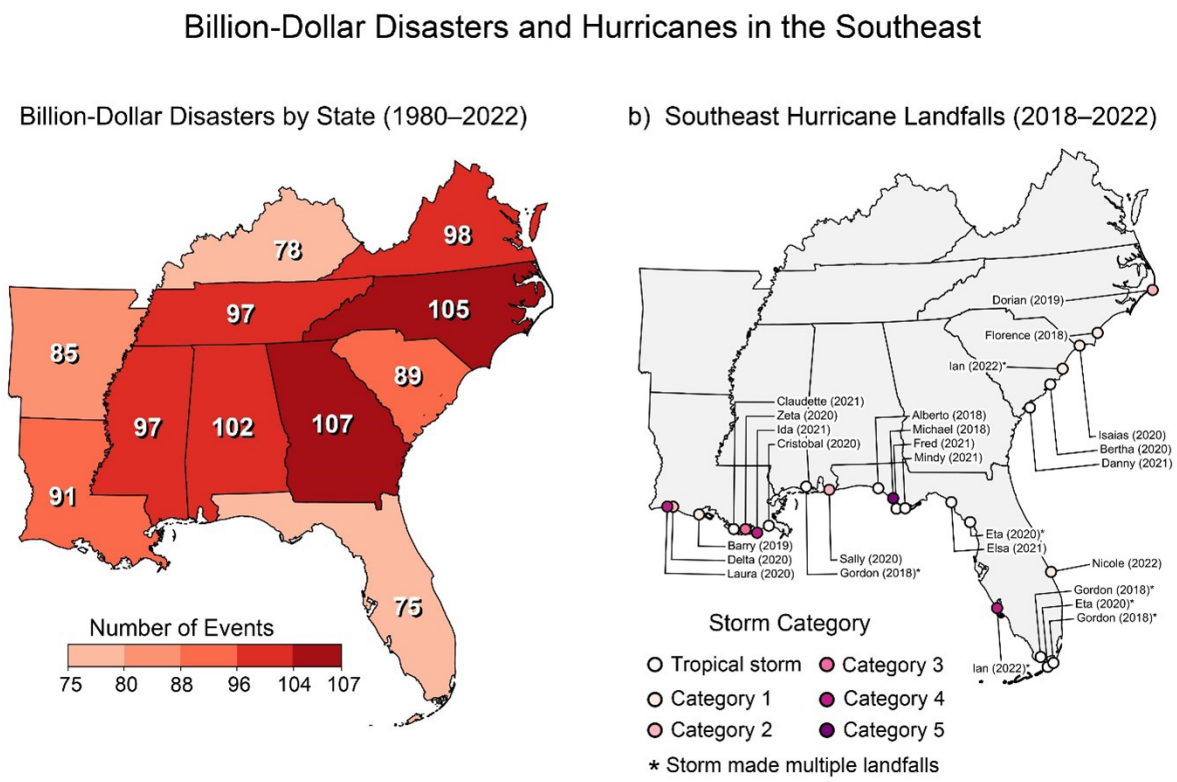

Figure X.X. Billion-dollar disasters and hurricanes in the Southeast (2018-2022): (a) billion-dollar disaster by state (b) Southeast hurricane landfalls (Jay et al., 2023).

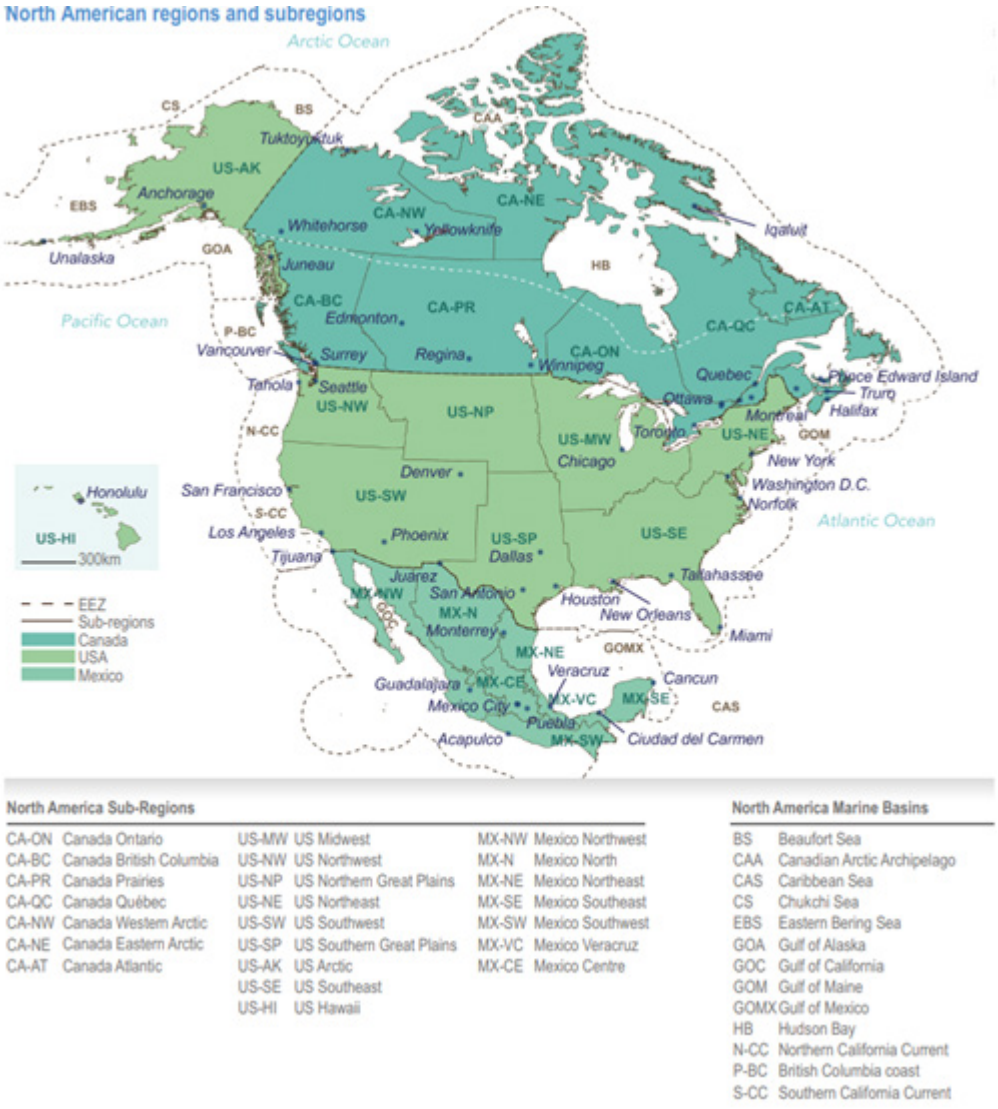

Figure X.Y. North America subregions as depicted in IPCC's (2022) Figure 14.1.

References:

IPCC. (2022). Climate Change 2022: Impacts, Adaptation and Vulnerability. Contribution of Working Group II to the Sixth Assessment Report of the Intergovernmental Panel on Climate Change [Pörtner, H.- O., Roberts, D. C., Tignor, M., Poloczanska, E. S., Mintenbeck, K., Alegría, A., Craig, M., Langsdorf, S., Löschke, S., Möller, V., Okem, A., & Rama, B. (Eds.)]. Cambridge University Press. Cambridge University Press, Cambridge, UK and New York, NY, USA, 3056 pp., https://doi.org/10.1017/9781009325844

Jay, A. K., Crimmins, A. R., Avery, C. W., Dahl, T. A., Dodder, R. S., Hamlington, B. D., Lustig, A., Marvel, K., Méndez-Lazaro, P. A., Osler, M. S., Terando, A., Weeks, E. S., & Zycherman, A. (2023). Ch. 1. Overview: Understanding risks, impacts, and responses. In: Fifth National Climate Assessment. Crimmins, A. R., Avery, C. W., Easterling, D. R., Kunkel, K. E., Stewart, B. C., & Maycock, T. K. (Eds.) U.S. Global Change Research Program, Washington, DC, USA. https://doi.org/10.7930/NCA5.2023.CH1

Temperature Hazards

Future Conditions: Extreme Heat and Cold

Our assessment of future vulnerability to extreme temperatures begins with a review of the consensus of the major general circulation model (GCM) output for mean temperature. From that point, more specific estimates of extreme temperatures might be possible. NCA5 (Jay et al., 2023) notes that all U.S. regions are experiencing increasing temperatures and longer-lasting heatwaves. Concurrently, cascading and compounding negative impacts of the more frequent and severe extreme events are increasing nationwide, such as via heat-related illnesses and mortality, increased loss from storms, lengthening droughts, and more frequent and severe wildfires (Jay et al., 2023), all of which exacerbate societal inequalities.

The observed temperature record of the U.S. Southeast region is characterized by a warm peak during the 1930s and 1940s, followed by a cool period in the 1960s and 1970s, with temperatures increasing again since 1970 (NCA, 2017). While the southeastern U.S., including Louisiana, exhibited little or no change in surface temperature from 1986 to 2015 relative to 1901 to 1960 (Wuebbles et al., 2017; their Figure 1.3) and little overall warming over the 20th century (Frankson et al., 2017), the 1986 to 2016 period was up to 1°F warmer than the 1901 to 1960 period in Louisiana, with most of the Louisiana warming concentrated in the northeastern and coastal southeastern parts of the state (Vose et al., 2017). This warming was much less than that reported in most of the northern and western United States.

More recently, Kunkel et al. (2022) reiterates a similar historical temperature climatology for Louisiana, while also noting that Louisiana temperatures have increased by only 0.5°F since 1900 – less than one-third of that experienced by the contiguous U.S. as a whole – but with the 2016 to 2020 period being the warmest five-year interval in that period. The most recent numbers from NCA5 (Jay et al., 2023) would place this amount of warming as only one-fifth of that experienced by the contiguous United States. The spatial distribution of observed warming by season for the U.S. is shown in Figure X.M, and overall warming across the terrestrial and marine Earth is shown in Figure X.N. NCA5 (Jay et al., 2023) also notes the increasing stress from extreme heat on human health in the U.S. Southeast, including Louisiana. The confidence in these conclusions by NCA4 (2017) was reported as “very high,” and NCA5 (Jay et al., 2023) forecasts that with projected changes in annual surface temperature compared to the present-day (1991–2020) under a global warming level of 3.6°F (2°C) above preindustrial levels, the U.S. Southeast would experience six more days per year with temperatures exceeding 100°F.

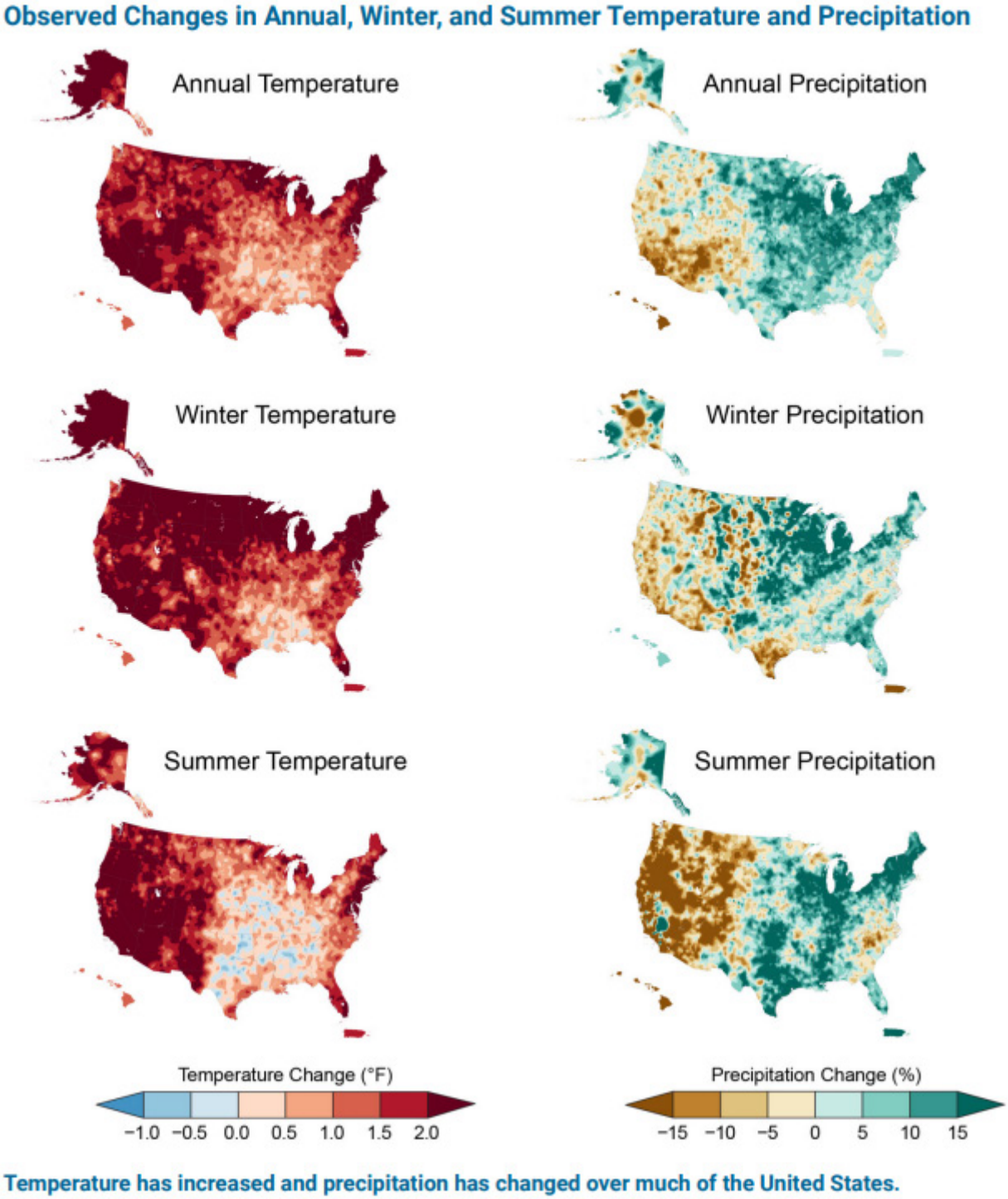

Figure X.M. Spatial distribution of observed temperature and precipitation changes for the U.S., as represented by the 2002 through 2021 means minus the 1901 to 1960 means & Source: Figure 2.4 in Jay et al., 2023.

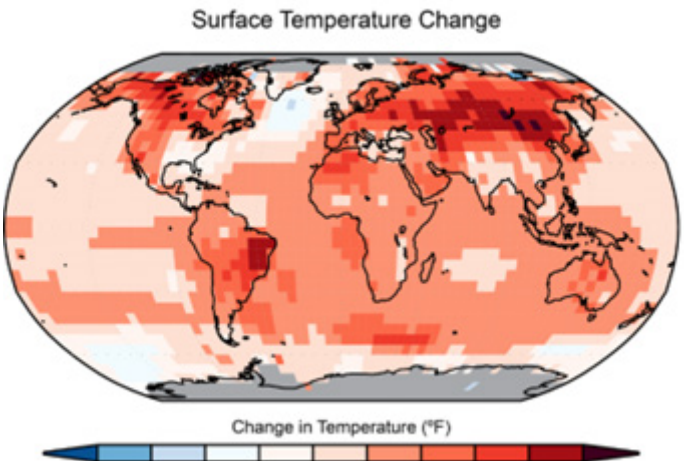

Fig X.N: Surface temperature change (in °F) for the period 1986–2015 relative to 1901–1960 from the NOAA National Centers for Environmental Information's (NCEI) surface temperature product. (Figure source: updated from Vose et al. (2012))

NCA5 summarizes other research that bases outcomes on current policies by estimating a global warming of around 2.6°C (ranging from 2°–3.7°C) by 2100. The prevailing scientific literature suggests that by 2050, warming is expected to intensify for the southeastern U.S., including Louisiana. More specifically, NCA4 (2017) says that "statistically significant warming is projected for all parts of the U.S. throughout the [21st] century...warming rates (and spatial gradients) are greater at higher latitudes." The confidence in these conclusions by NCA4 (2017) is reported as "high." The additional evapotranspiration in the Southeast due to warming, will allow additional condensation and cloud cover, which will in turn suppress further warming. This contrasts with other regions in which moisture is not as abundant. In those regions, the extra energy input will result in higher increases in temperature.

NCA4 (2017) analyzed modeled changes in mean temperature by 2036–2065, as compared to 1976–2005. Two scenarios were chosen, to conform to those used by the Intergovernmental Panel on Climate Change. The higher radiative forcing scenario (Representative Concentration Pathway (RCP) 8.5 (suggesting an increase of 8.5 Watts per square meter of energy loading)) would result in a mean temperature increase of 2–6°F in Louisiana across the two 30-year periods (Figure X.O; same as Figure 6.7 in NCA4 (2017)), with a mean Increase across the U.S. Southeast of 4.30°F. The lower forcing scenario (RCP4.5) would result in 2–4°F increases in mean temperature across Louisiana, with a mean increase by mid-century of 3.40°F for the U.S. Southeast region. Under a higher emissions pathway, historically unprecedented warming is projected for Louisiana by the end of the 21st century (Frankson et al., 2017).

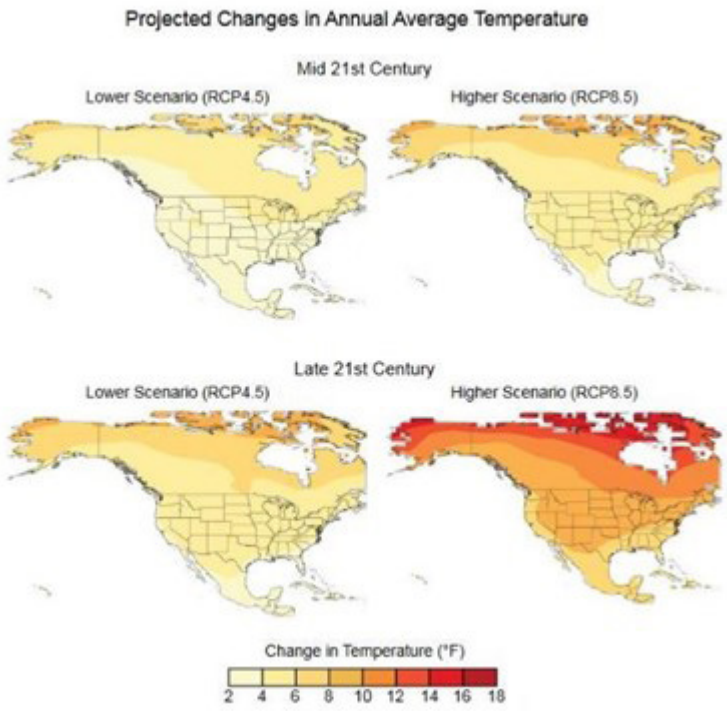

Fig X.O: Projected changes in annual average temperatures (°F). Changes are the difference between the average for mid-century (2036–2065; top) or late-century (2070–2099, bottom) and the average for near-present (1976–2005) (Source: CICS-NC and NOAA NCEI).

NCA4 (2017) also projected changes to temperature extremes. RCP8.5 would increase the temperature of the coldest day of the year by 2–4°F and the warmest day of the year by 2–4°F in Louisiana, except for the extreme coastal southeast, where increases of 0–2°F are projected (Figure X.P – Same as Figure 6.8 in Vose et al., 2017). Mean increases for the U.S. Southeast region are 4.97°F and 5.79°F, respectively (Vose et al., 2017). Louisiana might expect 20 to 30 more days annually with temperatures above 90°F and 1 to 20 fewer days per year with freezing temperatures by the 2036–2065 period (Figure X.Q – same as Figure 6.9 in Vose et al., 2017). Larger increases in extreme high temperature frequency are expected in inland regions, including northern Louisiana. Much smaller increases in the mean number of days per year exceeding 95°F are expected in coastal Louisiana, but these increases are also substantial on a percentage basis. The confidence in these conclusions by NCA4 (2017) about changes to U.S. extreme temperature days is reported as "very high." NCA4 (2017) does not examine the changes to extremes that would occur in an RCP4.5 scenario.

While at the time of this writing, textual detailed projections by U.S. regions are not yet available in Jay et al. (2023), figures from that source are available. Figure X.R (reproduced from Jay et al., 2023) shows that extreme temperature increases will burden households inequitably in much of the U.S. Southeast, including Louisiana, and that Louisiana rivals all of the other U.S. southeastern states in the projected increase in frequency of days at or above 95°F by 2050.

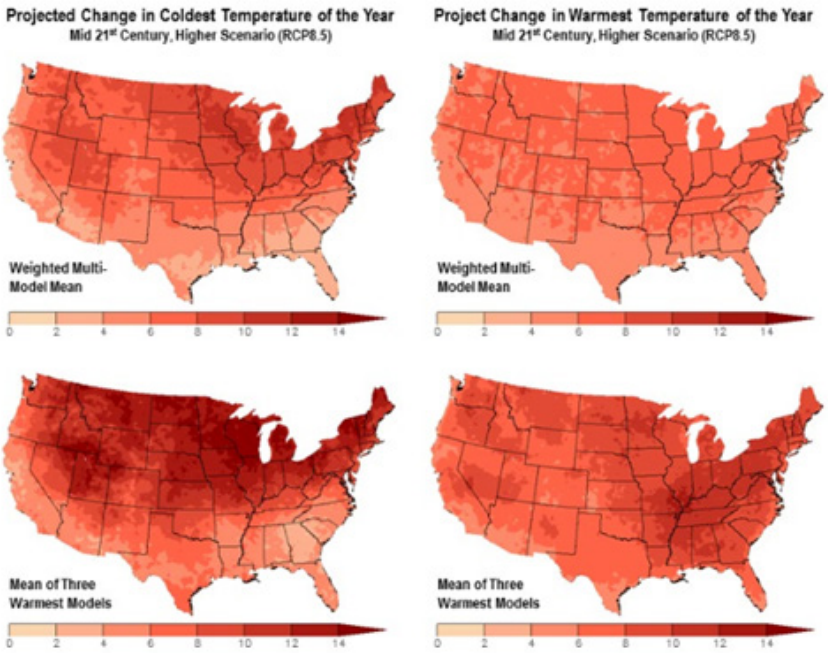

Figure X.P: Projected changes in the coldest and warmest daily temperatures (°F) of the year in the contiguous United States. Changes are the difference between the average for mid-century (2036–2065) and the average for near-present (1976–2005) under the high-emission scenario (RCP8.5) (Source: CICS-NC and NOAA NCEI)

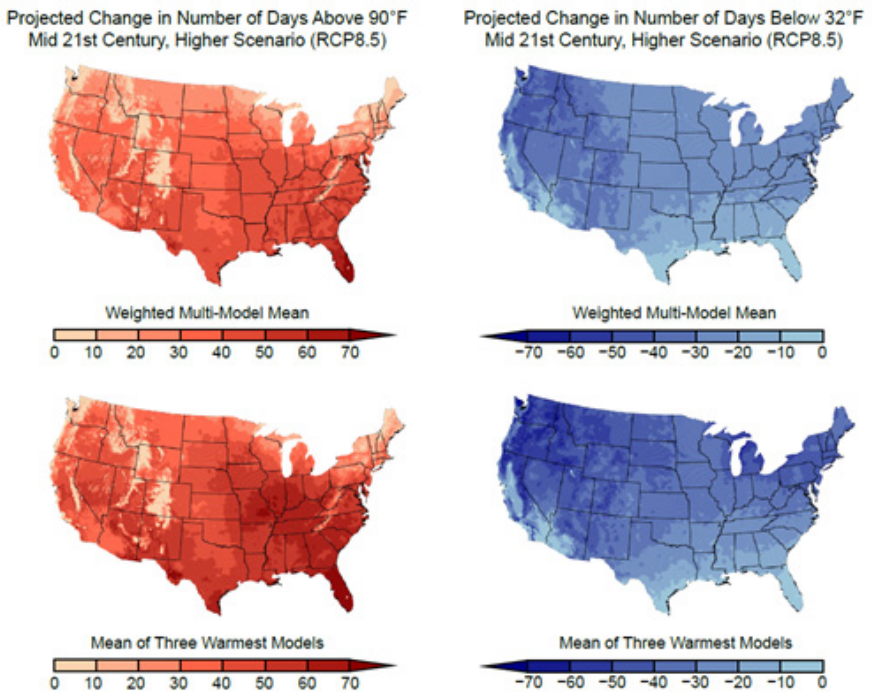

Figure X.O: Projected changes in the number of days per year with a maximum temperature above 90°F and a minimum temperature below 32°F in the contiguous United States. Changes are the difference between the average for mid-century (2036–2065) and the average for near-present (1976–2005) under the high-emission scenario (RCP8.5) (Figure source: CICS-NC and NOAA NCEI)

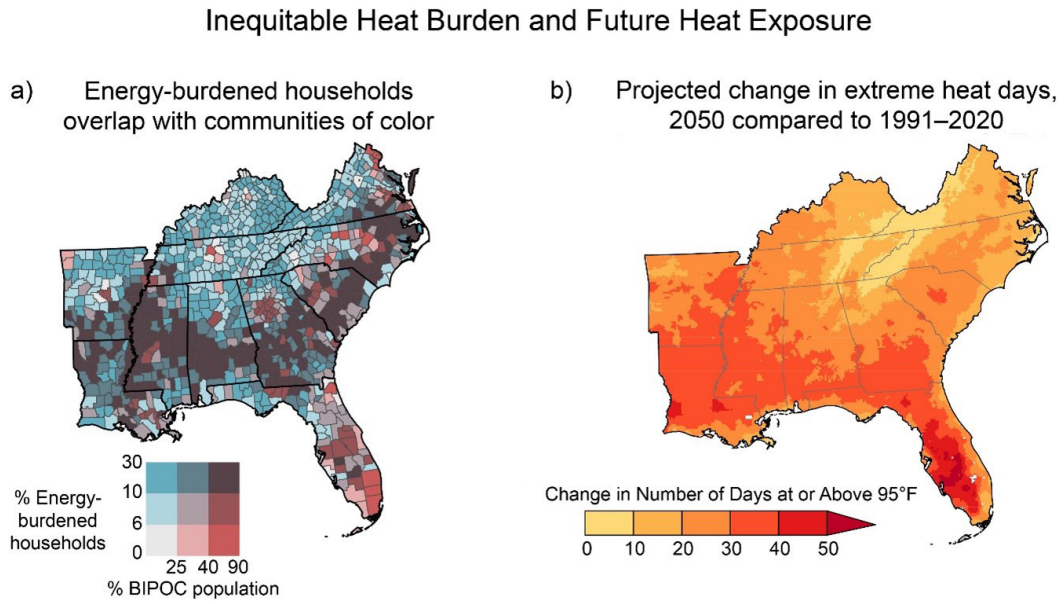

Figure X.R. Energy-burdened households relative to BIPOC populations, and projected change in the number of days with temperatures exceeding 95°F (Figure 22.9 in Jay et al., 2023).

Our study considers a 20 percent increase by the year 2050 in the days per year having maximum temperature exceeding 95°F, based on the data in NCA4 by Vose et al. (2017; their Figure 6.9) and the information in Figures X.P, X.Q, and X.R, although the Vose et al. (2017) figure used 90°F as the threshold rather than the 95°F used in the historical analysis (Mostafiz et al., 2022). According to the Texas A&M's Southern Regional Climate Center "Climate Data Portal," a total of 652 days between 1991 and 2020 (i.e., 21.7 per year) and 261 days between 2011 and 2020 (i.e., 26.1 per year) reached or exceeded 95°F in Baton Rouge (station KBTR). At KSHV, the respective numbers are 1277 and 520 (42.6 and 52.0 per year, respectively). At KMSY, the respective numbers are 508 and 243 (16.9 and 24.3 per year, respectively). If approximately 35 more days per year have a temperature of at least 95°F in Louisiana by 2050, our projection of a 20 percent increase in extreme hot days may be unduly conservative. And others (e.g., Twumasi et al., 2020) project rises in sea level near the Louisiana coast that promote abrupt, strong warming. Nevertheless, the unavailability (at this writing) of textual information in Jay et al. (2023) that explains the rationale and caveats behind their Figure 22.9 leaves us uncomfortable with more aggressive temperature projections than we used for the 2019 update to the Louisiana State Hazard Mitigation Plan. The 20 percent increase used in Mostafiz et al. (2022) passed through the peer review process.

As described in Mostafiz et al. (2020), changes to the extreme cold temperature hazard were assumed to parallel the projected changes to the annual mean frequency of sub- 0°C days. Vose et al. (2017; their Figure 6.9) also estimated such changes. Thus, the number of days per year below 32°F was assumed to decrease by 20 percent by 2050. The 20 percent decrease used in Mostafiz et al. (2020) passed through the peer review process.

References:

Frankson, R., Kunkel, K., & Champion, S. (2017). Louisiana State Summary. NOAA Technical Report NESDIS 149-LA, 4 pp. https://statesummaries.ncics.org/chapter/la/

Hoffman, J. S., McNulty, S. G., Brown, C., Dello, K. D., Knox, P. N., Lascurain, A., Mickalonis, C., Mitchum, G. T., Rivers III, L., Schaefer, M., Smith, G. P., Camp, J. S., & Wood, K. M. (2023). Ch. 22. Southeast. In: Fifth National Climate Assessment. Crimmins, A. R., Avery, C. W., Easterling, D. R., Kunkel, K. E., Stewart, B. C., & Maycock, T. K. (Eds.) U.S. Global Change Research Program, Washington, DC, USA. https://doi.org/10.7930/NCA5.2023.CH22
Jay, A. K., Crimmins, A. R., Avery, C. W., Dahl, T. A., Dodder, R. S., Hamlington, B. D., Lustig, A., Marvel, K., Méndez-Lazaro, P. A., Osler, M. S., Terando, A., Weeks, E. S., & Zycherman, A. (2023). Ch. 1. Overview: Understanding risks, impacts, and responses. In: Fifth National Climate Assessment. Crimmins, A. R., Avery, C. W., Easterling, D. R., Kunkel, K. E., Stewart, B. C., & Maycock, T. K. (Eds.) U.S. Global Change Research Program, Washington, DC, USA. https://doi.org/10.7930/NCA5.2023.CH1

Kunkel, K. E., Frankson, R., Runkle, J., Champion, S. M., Stevens, L. E., Easterling, D. R., Stewart, B. C., McCarrick, A., & Lemery, C. R. (Eds.). (2022). State climate summaries for the United States 2022: Louisiana. NOAA Technical Report NESDIS 150. NOAA/NESDIS, Silver Spring, MD. https://statesummaries.ncics.org/chapter/la/

Mostafiz, R. B., Friedland, C., Rohli, R. V., Gall, M., Bushra, N., & Gilliland, J.M. (2020). Census-block-level property risk estimation due to extreme cold temperature, hail, lightning, and tornadoes in Louisiana, United States. Frontiers in Earth Science (Lausanne), 8, Art. No. 601624. https://doi.org/10.3389/feart.2020.601624

Mostafiz, R.B., Rohli, R. V., Friedland, C. J., Gall, M., & Bushra, N. (2022). Future crop risk estimation due to drought, extreme temperature, hail, lightning, and tornado at the census tract level in Louisiana. Frontiers in Environmental Science, 10, 919782. https://doi.org/10.3389/fenvs.2022.919782

Twumasi, Y. A., Merem, E. C., Namwamba, J. B., Ayala-Silva, T., Okwemba, R., Mwakimi, O. S., Abdollahi, K., Lukongo, O. E. B., LaCour-Conant, K., Tate, J., & Akinrinwoye, C. O. (2020). Modeling the risks of climate change and global warming to humans settled in low elevation coastal zones in Louisiana, USA. Atmospheric and Climate Sciences, 10(3), 298–318. https://doi.org/10.4236/acs.2020.103017

Vose, R.S., Arndt, D., Banzon, V. F., Easterling, D. R., Gleason, B., Huang, B., Kearns, E., Lawrimore, J. H., Menne, M. J., Peterson, T. C., Reynolds, R. W., Smith, T. M., Williams, C. N., & Wuertz, D. L. (2012). NOAA's merged land-ocean surface temperature analysis. Bulletin of the American Meteorological Society 93, 1677–1685, https://doi.org/10.1175/BAMS-D-11-00241.1

Vose, R. S., Easterling, D. R., Kunkel, K. E., LeGrande, A. N., & Wehner, M. F. (2017). Temperature changes in the United States. In: Climate Science Special Report: Fourth National Climate Assessment, Volume I [Wuebbles, D. J., Fahey, D. W., Hibbard, K. A., Dokken, D. J., Stewart, B. C., & Maycock, T. K. (Eds.)]. U.S. Global Change Research Program, Washington, DC, USA, pp. 185-206, https://doi.org/10.7930/J0N29V45

Wuebbles, D. J., Easterling, D. R., Hayhoe, K., Knutson, T., Kopp, R. E., Kossin, J. P., Kunkel, K. E., LeGrande, A. N., Mears, C., Sweet, W. V., Taylor, P. C., Vose, R. S., & Wehner, M. F. (2017). Our globally changing climate. In: Climate Science Special Report: Fourth National Climate Assessment, Volume I [Wuebbles, D. J., Fahey, D. W., Hibbard, K. A., Dokken, D. J., Stewart, B. C., & Maycock, T. K. (Eds.)]. U.S. Global Change Research Program, Washington, DC, USA, pp. 35-72, https://doi.org/10.7930/J08S4N35

Future Conditions: Drought and Wildfire

The Louisiana droughts and wildfires of 2023 will remain etched in the minds of many for a long time. In fact, the term "flash drought" (Rakkasagi et al., 2023) has recently come into the lexicon to refer to relatively sudden onset of impacts from drought, which come with increased risk as the world continues to warm (Christian et al., 2023). Regardless of the speed of onset, impacts of such droughts are far reaching. For example, Figure 22.16 from Jay et al. (2023) highlights the effects of navigation lock closure on the Calcasieu River (Figure Z.Z).

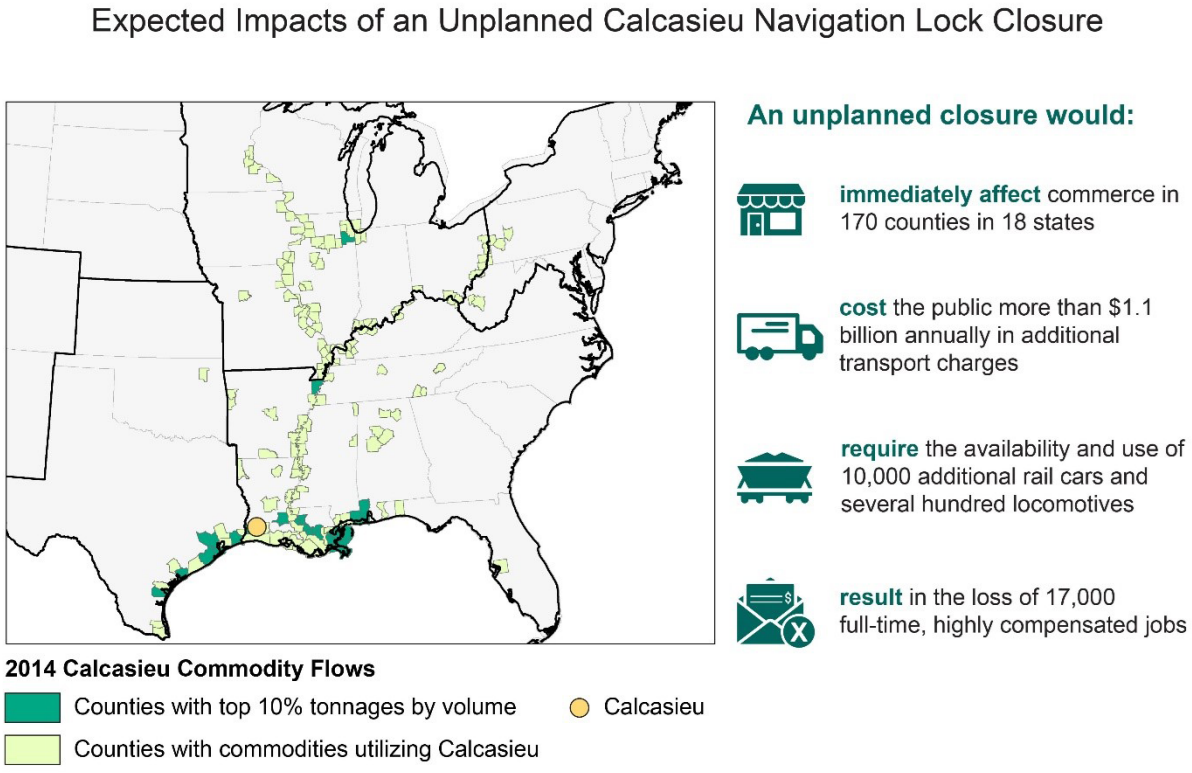

Figure Z.Z. Expected impacts of an unplanned Calcasieu Navigation Lock closure (Jay et al., 2023)

Nevertheless, until the detailed information from Jay et al. (2023) becomes available, I definitive study on future conditions of drought and wildfire in the U.S. remains the Fourth National Climate Assessment (NCA4, 2017). The Drought, Floods, and Wildfire section of that report (Wehner et al., 2017) concludes that:

"The human effect on recent major U.S. droughts is complicated. Little evidence is found for a human influence on observed precipitation deficits, but much evidence is found for a human influence on surface soil moisture deficits due to increased evapotranspiration caused by higher temperatures."

Wehner et al. (2017) suggest that by 2050, daily precipitation will increase by 9–13 percent in Louisiana, with higher increases corresponding to the higher radiative forcing scenario. The report also uses dynamically downscaled model output to find that, for the U.S. in the higher forcing scenario, a more extreme precipitation climate is to be expected by 2100. This includes substantial increases in the frequency of "no precipitation" and the (present) zero-to-tenth-percentile precipitation daily totals, sharp increases in the frequency of days having a greater than 90th percentile of precipitation, and decreases in every other decile of precipitation totals.

The projected increases in temperature and precipitation, and the seasonality of each, would induce changes in soil moisture, which in turn would cause changes in drought and wildfire. Therefore, it is appropriate to search the literature for projected changes in soil moisture by mid-century. Wehner et al. (2017) acknowledge that projections of seasonal precipitation deficits lack confidence. Louisiana precipitation is expected to change little by 2100 (Figure Y.A; Easterling et al., 2017, their Figure 7.5), enhanced evapotranspiration caused by increased temperatures may result in drying soils by 2100 over much of the continental U.S., including Louisiana, at least under the higher radiative forcing and emissions scenario (Figure Y.B; Wehner et al., 2017; their Figure 8.1).

These changes will impact soil moisture availability in Louisiana. Specifically, in Louisiana, winter, spring, and summer soil moisture decreases, made with a "medium" degree of confidence, are projected to be large relative to natural variability (Wehner et al., 2017). For these reasons, an increase in drought hazard of 25 percent was assumed for the state by 2050.

Soil moisture changes could be expected to produce changes in wildfire vulnerability. However, because the Fourth NCA focuses on the western U.S. in its discussion of wildfire, other sources must be used to assess the threat to Louisiana by 2050. Prestemon et al. (2016) used three general circulation models and three IPCC-based emission scenarios to assess future conditions of wildfire in the U.S. Southeast; the study concluded that median annual area affected by lightning-ignited wildfire will increase by 34 percent, and that total wildfire will increase by 4 percent by 2056–60 compared with the years 2016–2020.

A few other studies have been conducted in the last 15 years to make projections to changes in wildfire vulnerability. For such purposes, the Keetch-Byram Drought Index (KBDI), which is calculated based on observed or simulated changes in maximum temperature and precipitation, is most useful. The KBDI was developed by the U.S. Forest Service using a water balance approach. Specifically, it examines the relationship of modeled evapotranspiration (driven largely by temperature and latitude, the latter of which controls sun angle and number of hours of daylight) to precipitation in the organic matter on a forest floor and in the highest soil layers. The KBDI represents the number of millimeters of precipitation required to saturate the soil (i.e., reduce the KBDI to zero). Values from 0 to 200 indicate minimal wildfire threat, with values of 200 to 400 suggesting that the lower litter layer is drying and beginning to be susceptible to drought. Values from 400 to 600, which are more typical of late summer and early autumn, indicate that there is a moderate burn potential. Values of 600 to 800 are associated with more severe drought and active potential for burning.

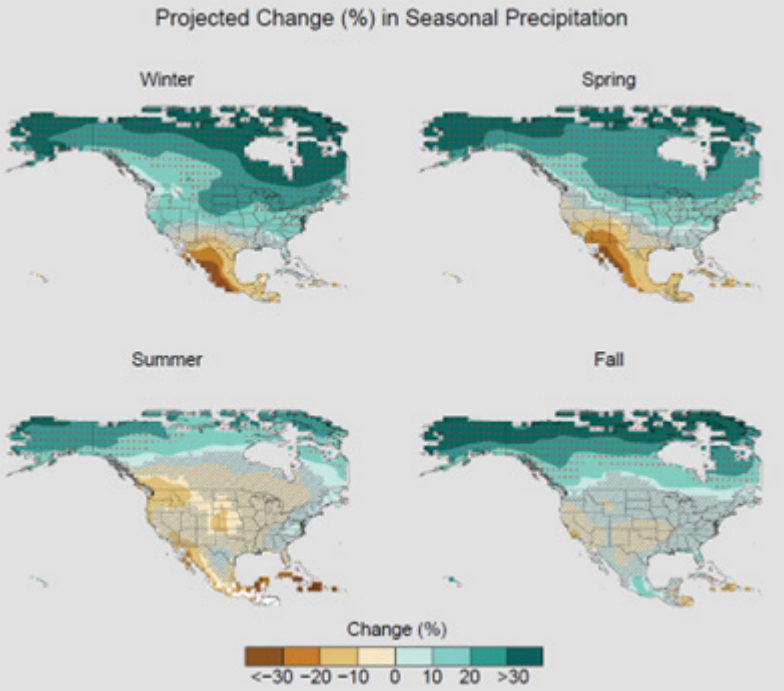

Figure Y.A: Projected change (%) in total seasonal precipitation from CMIP5 simulations for 2070–2099 (Source: NOAA NCEI)

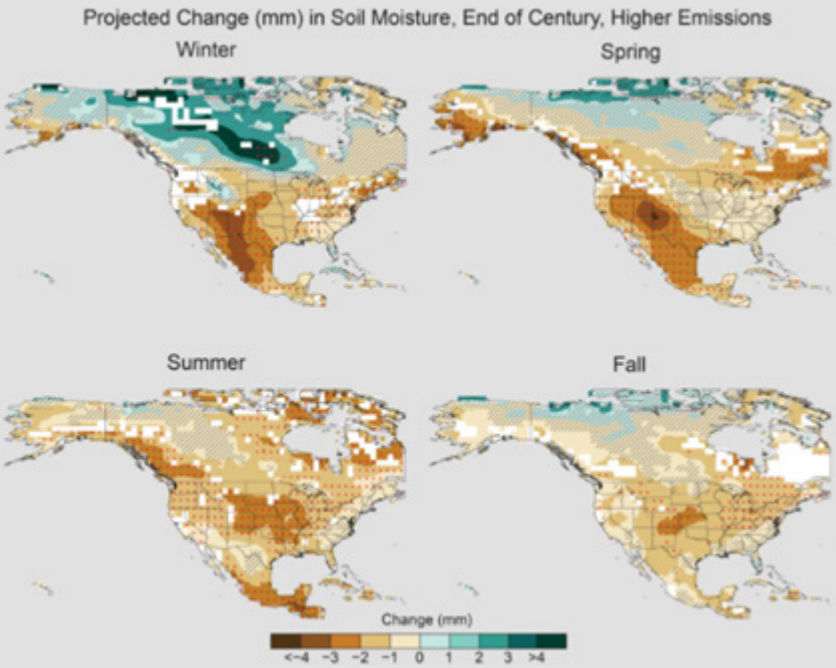

Figure Y.B. Projected end of the 21st century weighted CMIP5 multimodel average percent changes in near surface seasonal soil moisture under the higher scenario (RCP8.5). Stippling indicates that changes are assessed to be large compared to natural variations. Hashing indicates that changes are assessed to be small compared to natural variations. Blank regions (if any) are where projections are assessed to be inconclusive (Appendix B). (Source: NOAA NCEI and CICS-NC).

Liu et al. (2009) modeled seasonal changes to the KBDI (Figure Y.C) using the A2a scenario – the "non-fossil-intensive" variety of the "A2" scenario that had been used by NCA before its Fourth Assessment Report. The A2a scenario assumed that global population surpasses 10 billion by 2050, with relatively slow economic and technological development, creating global CO_2 mixing ratios of 575 parts per million (ppm) by 2050 and 870 ppm by 2100 (compared to the current 407 ppm). Validation of output from four general circulation models for global climate for the 1961–1990 period led Liu et al. (2009) to conclude that the Hadley Centre climate model version 3 (Pope et al., 2000) is most effective for simulating global KBDI for the 2070–2100 period. Figure Y shows those projected changes to the KBDI (2070–2100 minus 1961–1990) for the United States. In autumn and winter (September through February), decreases of 50–150 mm per three-month period were forecasted in Louisiana, while in March through May and June through August decreases of 200–250 mm per three-month period were projected in Louisiana.

The midpoint of the time series of the projection by Liu et al. (2009) is 2085, so we assumed that half of the projected changes in KBDI will occur by 2050. Thus, decreases of 25–75 mm per three-month period (or 8–25 mm per month, with 17 mm per month as the midpoint) are projected for each month from September through February in Louisiana by 2050. Decreases of 100–125 mm per three-month period (or 33–42 mm per month, with 38 mm per month as the midpoint) are projected for each month

from March through August in Louisiana by 2050 (Table 1). Recent research (Krueger et al., 2017) suggests that the fraction of available water (FAW) is a better predictor of large growing-season wildfires than the KBDI. FAW is calculated as the ratio of plant available water to soil water capacity. But FAW has not yet been projected as confidently to 2050 as precipitation. Other research from northern Europe (Bakke et al., 2021) points to shallow volumetric soil water anomaly as the dominant wildfire predictor; as remotely-sensed data become more precise, such a variable may become a more appropriate indicator of wildfire likelihood. Yu et al. (2023) found that regional-climate-model-based changes in the mean number of days that exceed the 95th percentile of four fire danger indices to 2100 is higher in the south-central U.S., which includes Louisiana, than elsewhere in the continental United States.

To provide more detail for Louisiana based on Liu et al.'s (2009) results, we collected average monthly precipitation data for 31°°N, 91.5°°W from the Web-based, Water-Budget, Interactive, Modeling Program (WebWIMP, http://climate.geog.udel.edu/~wimp/wimp_map_input.php). Results suggest that decreases in soil moisture in the upper layers of 12.2 percent (February) to 46.1 percent (August) are projected.

Based on these model results and other recent research which suggests a future increase in lightning-ignited wildfire for some parts of the world, though not necessarily the U.S. Southeast (Pérez-Invernón et al., 2023), we project a 25 percent decrease in available moisture in the organic matter and uppermost soil layers and a 25 percent increase in wildfire occurrence across Louisiana by 2050. Our projections are not without their caveats. For example, these changes do not consider projected changes in global air temperature. According to NCICS (https://statesummaries.ncics.org/la), Louisiana's mean air temperature trends have not mimicked global temperature trends, as:

> "Louisiana has exhibited little overall warming in surface temperatures over the 20th century. However, under a higher emissions pathway, historically unprecedented warming is projected by the end of the 21st century."

The changes described here assume no change in temperature by 2050 from current values. Nor do they consider the precipitation changes expected to replenish the soil layers during wet times but also desiccate the soil more rapidly during the lengthening dry periods. And projections for increases in wildfire in the western U.S. are more aggressive 50 percent, albeit from the 2001–2010 to 2050–2059 period (Liu et al., 2021). Thus, despite the fact that our use of a 25 percent increase in wildfire occurrence has passed peer review (Mostafiz et al., 2022), caution should be exercised in our interpretation of the results.

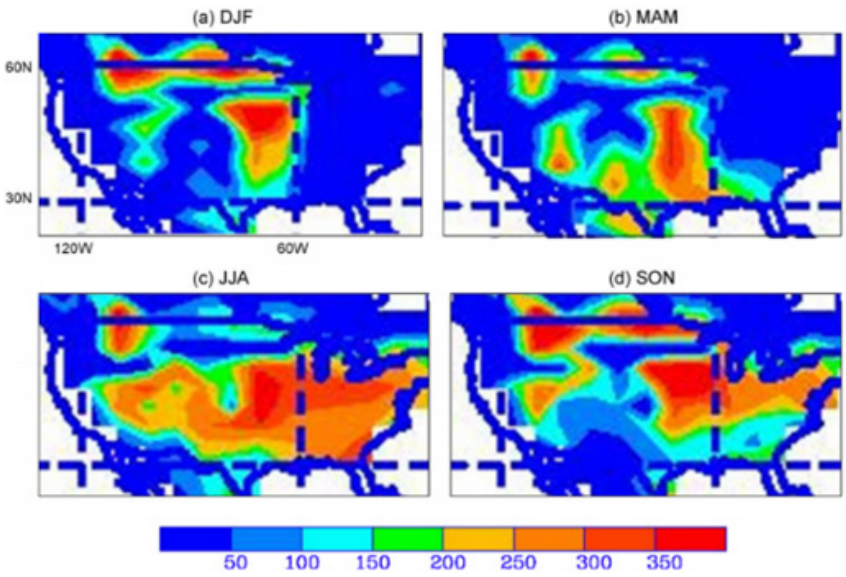

Figure Y.C: Projected changes to KBDI (mm) by annual quarter (Liu et al., 2009)

Table 1. Current monthly precipitation and projected decrease in KBDI and available water for precipitation by 2050, for 31°°N, 91.5°°W.

Month	Mean current precipitation (mm)	Projected decrease (mm) in available moisture in upper litter layers (KBDI)	Projected decrease in available water as a percentage of current precipitation (%)
January	133.8	17	12.7
February	139.5	17	12.2
March	159.7	38	23.8
April	130	38	29.2
May	132.6	38	28.7
June	95.6	38	39.7
July	94	38	40.4
August	82.4	38	46.1
September	80.1	17	21.2
October	74.1	17	22.9
November	113	17	15.0
December	128.6	17	13.2

Regarding risk, the most recent research suggests that the impacts of drought on the agricultural sector in the U.S. Southeast (which includes parts of Louisiana) is up to 42.7 and 25.4 percent for maize and soybean, respectively (Nguyen et al., 2023).

Wildfire Risk Assessment:

Property loss due to wildfire is calculated as

$$L_{2050,i} = PV_{2050,i} \times p(f)_i \times p(d|f_i) \times d \times F_{2050,i}$$

where

$L_{2050,i}$ = projected annual preperty loss of census block i in 2050

$PV_{2050,i}$ = estimated total property (building + content) value of census block$i$ in 2050

$p(f)_i$ = probability of fire occurrence of census block i

$p(d|f)_i$ = conditional probability of damage of census block i when a fire occurs

d = average percent of damage for each damaged building

$F_{2050,i}$= future hazard multiplication factor for census block i in 2050

We summed the probability of large fires from FSim and calculated the annual probability of small fires using FPA data. Based on LDAF records 2007–2017, 12,979 Louisiana residences have been threatened by fire. Of these, 389 were damaged and 12,590 were protected, a relative damage frequency of 0.03. Therefore, p(d|f) = 0.03. The losses were calculated, assuming that 3% of buildings exposed to fire were damaged, with a relative loss of 5% of the value of each building.

References

Bakke, S. J., Wanders, N., van der Wiel, K., & Tallaksen, L. M. (2021). A data-driven prediction model for Fennoscandian wildfires. Hydrology and Earth System Science Discussion [Preprint], https://doi.org/10.5194/nhess-2021-384

Christian, J. I., Martin, E. R., Basara, J. B., Furtado, J. C., Otkin, J. A., Lowman, L. E., Hunt, E. D., Mishra, V., & Xiao, X. (2023). Global projections of flash drought show increased risk in a warming climate. Communications Earth & Environment, 4(1), 165. https://doi.org/10.1038/s43247-023-00826-1

Easterling, D. R., Arnold, J. R., Knutson, T., Kunkel, K. E., LeGrande, A. N., Leung, L. R., Vose, R. S., Waliser, D. E., & Wehner, M. F. (2017). Ch. 7: Precipitation Change in the United States. Climate Science Special Report: Fourth National Climate Assessment, Volume I. U.S. Global Change Research Program. https://doi.org/10.7930/J0H993CC

Krueger, E. S., Ochsner, T. E., Quiring, S. M., Engle, D. M., Carlson, J. D., Twidwell, D., & Fuhlendorf, S. D. (2017). Measured soil moisture is a better predictor of large growing-season wildfires than the Keetch-Byram Drought Index. Soil Science Society of America Journal, 81(3), 490–502. https://doi.org/10.2136/sssaj2017.01.0003

Liu, Y., Liu, Y., Fu, J., Yang, C. E., Dong, X., Tian, H., Tao, B., Yang, J., Wang, Y., Zou, Y., & Ke, Z. (2021). Projection of future wildfire emissions in western USA under climate change: Contributions from changes in wildfire, fuel loading and fuel moisture. International Journal of Wildland Fire, 31(1), 1–13. https://doi.org/10.1071/WF20190

Liu, Y., Stanturf, J. A., & Goodrick, S. L. (2009). Trends in global wildfire potential in a changing climate. Forest Ecology and Management, 259(4–5), 685–697. https://doi.org/10.1016/j.foreco.2009.09.002

Mostafiz, R. B., Rohli, R. V., Friedland, C. J., Gall, M., & Bushra, N. (2022a). Future crop risk estimation due to drought, extreme temperature, hail, lightning, and tornado at the census tract level in Louisiana. Frontiers in Environmental Science, 10, 919782. https://doi.org/10.3389/fenvs.2022.919782

Mostafiz, R. B., Friedland, C. J., Rohli, R. V., & Bushra, N. (2022b). Future property risk estimation for wildfire in Louisiana, USA. Climate, 10(4), Art. No. 49. https://doi.org/10.3390/cli10040049

Nguyen, H., Thompson, A., & Costello, C. (2023). Impacts of historical droughts on maize and soybean production in the southeastern United States. Agricultural Water Management, 281, https://doi.org/10.1016/j.agwat.2023.108237

Pérez-Invernón, F. J., Gordillo-Vázquez, F. J., Huntrieser, H., & Jöckel, P. (2023). Variation of lightning-ignited wildfire patterns under climate change. Nature Communications, 14(1), 739. https://doi.org/10.1038/s41467-023-36500-5

Pope, V., Gallani, M. L., Rowntree, P. R., & Stratton, R. A. (2000). The impact of new physical parameterizations in the Hadley Centre climate model: HadAM3. Climate Dynamics, 16, 123–146. https://doi.org/10.1007/s003820050009

Prestemon, J. P., Shankar, U., Xiu, A., Talgo, K., Yang, D., Dixon, E., McKenzie, D., & Abt, K. L. (2016). Projecting wildfire area burned in the south-eastern United States, 2011–60. International Journal of Wildland Fire, 25(7), 715–729. https://doi.org/10.1071/WF15124

Rakkasagi, S., Poonia, V., & Goyal, M. K. (2023). Flash drought as a new climate threat: drought indices, insights from a study in India and implications for future research. Journal of Water and Climate Change, 14(9), 3368–3384. https://doi.org/10.2166/wcc.2023.347

Wehner, M. F., Arnold, J. R., Knutson, T., Kunkel, K. E., & LeGrande, A. N. (2017). Droughts, floods, and wildfires. In: Climate Science Special Report: Fourth National Climate Assessment, Volume I [Wuebbles, D. J., Fahey, D. W., Hibbard, K. A., Dokken, D. J., Stewart, B. C., & Maycock, T. K. (eds.)]. U.S. Global Change Research Program, Washington, DC, USA, pp. 231–256. https://doi.org/10.7930/JOCJ8BNN

Yu, G., Feng, Y., Wang, J., & Wright, D. B. (2023). Performance of fire danger indices and their utility in predicting future wildfire danger over the conterminous United States. Earth's Future, 11(11), e2023EF003823. https://doi.org/10.1029/2023EF003823

Wind and Flood Hazards

Future Conditions: Tropical Cyclones

Future vulnerability to tropical cyclones has been a topic of intense scrutiny in scholarly literature of the last decade. On the one hand, several natural processes linked to enhancement of tropical cyclones might seem to become more favored in a warming world. For example, warming would increase the geographic extent at which water temperatures are high enough to provide the energy required to support or enhance a tropical cyclone and/or lead to a longer period in the year in which tropical cyclones may occur. Also, because the Earth's surface is anticipated to warm at a greater rate than the upper-level atmosphere, thermal turbulence and atmospheric instability would be enhanced, possibly leading to more evaporation from the surface. Atmospheric water vapor capacity would also increase under warmer conditions. Furthermore, a warming world could also be likely to cause a poleward retreat in the west-to-east-moving subtropical and polar front jet stream, both of which separate tropical air from much colder air. Because the jet streams shear the tops off developing tropical cyclones, their migration poleward would provide a more favorable environment for growth of tropical systems, unimpeded by the shear that might weaken them or carry them eastward across the Atlantic Ocean, away from Louisiana. These concerns are exacerbated by research that suggests a tight positive linkage between global temperature and tropical cyclone activity via feedback related to ocean mixing and transport, including rapid intensification (e.g., Sriver, 2010; Singh and Roxy, 2022).

On the other hand, simulation models do not necessarily agree that the frequency of tropical cyclones will increase in a warming world. Bengtsson et al. (2007) projected a 20 percent decrease in frequency by the end of the 21st century, including a 5–10 percent decrease in the Gulf of Mexico from the 20th to the 21st century. Ensemble modeling by Colbert et al. (2013) suggested that the weakening easterly trade winds under double CO_2 conditions (i.e., 720 ppm) by 2100 would decrease the frequency of tropical cyclones in the Gulf of Mexico by one to 1.5 per decade. Wang and Wu (2013) isolated the impacts of global warming from that attributable to the Atlantic Multidecadal Oscillation (AMO) – a naturally-occurring warm-cold oscillation of Atlantic Ocean temperatures that began its most recent warm phase in 1995 – with the conclusion that global warming causes an eastward shift in the Atlantic tropical cyclone genesis zone, while the warm-phase AMO is responsible for basin wide enhancement. The implication is that frequency may decrease when the AMO flips back to the cold phase in the coming decades. Work summarized in the Fourth National Climate Program Assessment (Kossin et al., 2017) suggests that, with low confidence, the frequency of the most intense Atlantic tropical cyclones is projected to increase. More recently, Chand et al. (2022) concurred that global tropical cyclone

frequency would decrease under additional warming; while an increasing frequency trend in the North Atlantic basin has been noted over the last few decades, perhaps because of reduced aerosol forcing and other factors, these researchers otherwise found no statistically significant trend when an extended period of reconstructed observational data are considered.

The impact of global warming on the intensity of tropical cyclones, however, is a different matter. Bengtsson et al. (2007) projected no decreases, and perhaps a substantial increase, in the frequency of the most intense tropical cyclones. Tory et al. (2013) confirmed such projections with a new generation of models. More recent research on the topic generally seems to confirm the "increased intensity" conclusions of previous studies, with warning of additional dangers associated with the increased intensity of tropical cyclones under a warming global climate. For example, Moore et al. (2015) concurred with the previous conclusions, while also anticipating a decrease in the periodicity of the El Niño/Southern Oscillation, which is known to suppress Gulf-Caribbean-Atlantic tropical cyclone activity. The resulting increased interannual variability could leave people uncertain of the trend of the hazard. Walsh et al. (2016) projected increases in tropical cyclone precipitation intensities in addition to the changes previously discussed. Such precipitation could increase even farther inland than today. Sun et al. (2017) noted that the area of the tropical cyclone-induced high winds will increase under global warming scenarios. And Appendini et al. (2017) warned that the wave activity associated with tropical cyclones will likely increase in the northern Gulf of Mexico under global warming scenarios. The Fourth National Climate Assessment (Kossin et al., 2017) provides an ominous reminder that atmospheric scientists tend to be converging toward a conclusion on the matter:

> "Both theory and numerical modeling simulations generally indicate an increase in tropical cyclone (TC) intensity in a warmer world, and the models generally show an increase in the number of very intense TCs. For Atlantic and eastern North Pacific hurricanes and western North Pacific typhoons, increases are projected in precipitation rates (high confidence) and intensity (medium confidence)."

Most recently, Feng et al. (2023) and Garner (2023) are among those who have found increasing intensity in North Atlantic tropical cyclones in a warming world. Yet there is still marked uncertainty (Méndez-Tejeda &Hernández-Ayala, 2023). Thus, more work is needed, particularly under assumptions of less drastic increases in CO_2 emissions, with a focus on the middle of the 21st century rather than the end, and at the regional rather than the basin wide scale.

Scholars have also estimated the future impacts resulting from such a consensus of increases in intensity and/or frequency of the most intense tropical cyclones. While emphasizing the inherent uncertainty and difficulty with projecting the future tropical cyclone hazard, Knutson et al. (2010) cautiously projected no major macro-scale changes in tropical cyclone genesis location, tracks, duration, or areas of impact, but cautioned that the future vulnerability to tropical-cyclone-induced storm surge-related flooding will

increase due to sea level rise and coastal development. Ranson et al. (2014) used ensemble models to project a 63 percent increase in tropical cyclone damage in the North Atlantic basin – the highest increase of any basin in the world. Most recently, Petrolia et al. (2022) found that "FORTIFIED" coastal home construction reduces wind risk and insurance costs while increasing a home's value.

Regardless of projections of the impact of global warming on regional tropical cyclone activity, Louisiana will always be in a geographic position in which tropical cyclones may track. Any increased intensities in the future, even with decreased frequencies, are likely to enhance Louisiana's future vulnerability, given that the intense storms have enormous potential to devastate the physical, urban, agricultural, economic, and sociocultural infrastructure of our state. We project a 25 percent increase in the future vulnerability to tropical cyclones, with a near-certain expectation that Louisiana will experience another major tropical cyclone before mid-century.

References:

Appendini, C. M., Pedrozo-Acuña, A., Meza-Padilla, R., Torres-Freyermuth, A., Cerezo-Mota, R., López-González, J., & Ruiz-Salcines, P. (2017). On the role of climate change on wind waves generated by tropical cyclones in the Gulf of Mexico. Coastal Engineering Journal, 59(2), Art No. 1740001. https://doi.org/10.1142/S0578563417400010

Bengtsson, L., Hodges, K. I., Esch, M., Keenlyside, N., Kornblueh, L., Luo, J. J., & Yamagata, T. (2007). How may tropical cyclones change in a warmer climate? Tellus Series A – Dynamic Meteorology and Oceanography, 59A, 539–561. https://doi.org/10.1111/j.1600-0870.2007.00251.x

Chand, S. S., Walsh, K. J., Camargo, S. J., Kossin, J. P., Tory, K. J., Wehner, M. F., Chan, J. C. L., Klotzbach, P. J., Dowdy, A. J., Bell, S. S., Ramsay, H. A., & Murakami, H. (2022). Declining tropical cyclone frequency under global warming. Nature Climate Change, 12(7), 655–661. https://doi.org/10.1038/s41558-022-01388-4

Colbert, A. J., Soden, B. J., Vecchi, G. A., & Kirtman, B. P. (2013). The impact of anthropogenic climate change on North Atlantic tropical cyclone tracks. Journal of Climate, 26(12), 4088–4095. https://doi.org/10.1175/JCLI-D-12-00342.1

Feng, Z., Shi, J., Sun, Y., Zhong, W., Shen, Y., Lv, S., Yao., Y., & Zhao, L. (2023). Impact of global warming on tropical cyclone track and intensity: A numerical investigation. Remote Sensing, 15(11), 2763. https://doi.org/10.3390/rs15112763

Garner, A. J. (2023). Observed increases in North Atlantic tropical cyclone peak intensification rates. Scientific Reports, 13(1), 16299. https://doi.org/10.1038/s41598-023-42669-y

Knutson, T. R., McBride, J. L., Chan, J., Emanuel, K., Holland, G., Landsea, C., Held, I., Kossin, J. P., Srivastava, A. K., & Sugi, M. (2010). Tropical cyclones and climate change. Nature

Geoscience, 3, 157–163. https://doi.org/10.1038/ngeo779

Kossin, J. P., Hall, T., Knutson, T., Kunkel, K. E., Trapp, R. J., Waliser, D. E., & Wehner, M. F. (2017). Extreme storms. In: Climate Science Special Report: Fourth National Climate Assessment, Volume I [Wuebbles, D. J., Fahey, D. W., Hibbard, K. A., Dokken, D. J., Stewart, B. C., & Maycock, T. K. (Eds.)]. U.S. Global Change Research Program, Washington, DC, USA, pp. 257–276. https://doi.org/10.7930/J07S7KXX

Méndez-Tejeda, R., Hernández-Ayala, J. J. (2023). Links between climate change and hurricanes in the North Atlantic. PLOS Climate, 2(4), e0000186. https://doi.org/10.1371/journal.pclm.0000186

Moore, T.R., Matthews, H. D., Simmons, C., & Leduc, M. (2015). Quantifying changes in extreme weather events in response to warmer global temperatures. Atmosphere-Ocean, 53(4), 412–425. https://doi.org/10.1080/07055900.2015.1077099

Petrolia, D., Ishee, S., Yun, S., Cummings, R., & Maples, J. (2023). Do wind hazard mitigation programs affect home sales values? Journal of Real Estate Research, 45(2), 137–159. https://doi.org/10.1080/08965803.2022.2066249

Ranson, M., Kousky, C., Ruth, M., Jantarasami, L., Crimmins, A., & Tarquinio, L. (2014). Tropical and extratropical cyclone damages under climate change. Climatic Change, 127, 227–241. https://doi.org/10.1007/s10584-014-1255-4

Singh, V. K., & Roxy, M. K. (2022). A review of ocean-atmosphere interactions during tropical cyclones in the north Indian Ocean. Earth-Science Reviews, 226, 103967. https://doi.org/10.1016/j.earscirev.2022.103967

Sriver, R. L. (2010). Climate change: Tropical cyclones in the mix. Nature, 463(7284), 1032–1033. https://doi.org/10.1038/4631032a

Sun, Y., Zhong, Z., Li, T., Yi, L., Hu, Y. J., Wan, H. C., Chen, H. S., Liao, Q. F., Ma, C., & Li, Q. H. (2017). Impact of ocean warming on tropical cyclone size and its destructiveness. Scientific Reports, 7, Art. No. 8154. https://doi.org/10.1038/s41598-017-08533-6

Tory, K.J., Chand, S. S., McBride, J. L., Ye, H., & Dare, R. A. (2013). Projected changes in late-twenty-first-century tropical cyclone frequency in 13 coupled climate models from Phase 5 of the Coupled Model Intercomparison Project. Journal of Climate, 26(24), 9946–9959. https://doi.org/10.1175/JCLI-D-13-00010.1

Walsh, K. J. E., McBride, J. L., Klotzbach, P. J., Balachandran, S., Camargo, S. J., Holland, G., Knutson, T. R., Kossin, J. P., Lee, T. C., Sobel, A., & Sugi, M. (2016). Tropical cyclones and climate change. Wiley Interdisciplinary Reviews-Climate Change, 7(1), 65–89. https://doi.org/10.1002/wcc.371

Wang, R. F. & Wu, L. G. (2013). Climate changes of Atlantic tropical cyclone formation derived from twentieth-century reanalysis. Journal of Climate, 26(22), 8995–9005. https://doi.org/10.1175/JCLI-D-13-00056.1

Future Conditions: High Wind

Future frequency of high wind events is particularly difficult to predict, because high wind may accompany many different types of storms, each with their own distinct patterns of projected changes. *NCA4 (2017) is again the most comprehensive source that synthesizes recent research on the topic. That document reports:*

> "Climate models consistently project environmental changes that would putatively support an increase in the frequency and intensity of severe thunderstorms (a category that combines tornadoes, hail, and winds), especially over regions that are currently prone to these hazards, but confidence in the details of this projected increase is low."

More recent literature (Jung and Schindler, 2019) suggests that under the RCP8.5 scenario of future human activities, 10-m mean wind speed distributions increase in some parts of the world but decrease in others, including in much of the United States. But the mean wind speed changes may not necessarily be correlated with those of extremes. Meucci et al. (2020) projects a general increase in wind-driven wave heights under medium- and RCP8.5 scenarios. Even though the frequency of the most intense tropical cyclones and tornadoes is expected to increase, such events are rare. High-wind events are much more commonly linked to thunderstorms, for which there is presently little evidence of a major frequency change by mid-century. And with an increasing trend toward building wind resilient structures as they become more widely recognized as profitable (Petrolia et al., 2023), we estimate no change to future conditions.

Jung, C., & Schindler, D. (2019). Changing wind speed distributions under future global climate. Energy Conversion and Management, 198, 111841. https://doi.org/10.1016/j.enconman.2019.111841

Kossin, J. P., Hall, T., Knutson, T., Kunkel, K. E., Trapp, R. J., Waliser, D. E., & Wehner, M. F. (2017). Extreme storms. In: Climate Science Special Report: Fourth National Climate Assessment, Volume I [Wuebbles, D. J., Fahey, D. W., Hibbard, K. A., Dokken, D. J., Stewart, B. C., & Maycock, T. K. (Eds.)]. U.S. Global Change Research Program, Washington, DC, USA, pp. 257–276. https://doi.org/10.7930/J07S7KXX

Meucci, A., Young, I. R., Hemer, M., Kirezci, E., & Ranasinghe, R. (2020). Projected 21st century changes in extreme wind-wave events. Science Advances, 6(24), eaaz7295. https://doi.org/10.1126/sciadv.aaz7295

Petrolia, D., Ishee, S., Yun, S., Cummings, R., & Maples, J. (2023). Do wind hazard mitigation programs affect home sales values? Journal of Real Estate Research, 45(2), 137–159. https://doi.org/10.1080/08965803.2022.2066249

Future Conditions: Hail

Hail has been studied fairly comprehensively for temporal trends and relationship to global climate change. As was described in the severe thunderstorm future vulnerability section, several counteracting potential forces seem to be at work. Increases in surface temperatures, at a rate exceeding the increase in upper-atmospheric temperatures, would destabilize the atmosphere further. In other words, the warmed air at the surface would acquire increased buoyancy, allowing for enhancement in vertical cloud growth, assuming that adequate moisture is present, which would in turn support stronger and perhaps more frequent hail events. The energized atmosphere under global warming situations would also presumably provide more evaporation over the oceans, which would indeed contribute the moisture needed to produce the enhanced cumulonimbus clouds that would support hail-bearing thunderstorms. However, an atmosphere in which the poles warm more strongly than the tropical parts of the Earth might be expected to weaken the tropical-to-pole gradient of energy, and therefore weaken frontal boundaries separating the two, making hail-bearing thunderstorms less frequent and intense. Likewise, any increases in atmospheric temperature might be more likely to allow hail to melt partially or completely when precipitating, but with high uncertainty in projections of net changes in hailstone diameter (Raupach et al., 2021).

In China, observational reports of a decrease in both the number of hail days (Xie et al., 2008) and the size of hail (Ni et al., 2017) have been identified. In a follow up study, Xie et al. (2010) found no significant trends in hail size across five provinces analyzed, as increases in convective available potential energy (CAPE) – a thermodynamic indicator of severe thunderstorms that often produce hail – tended to be offset by an increase in the height of the freezing level, which would tend to oppose hail generation. These results generally support the notion that opposing meteorological factors are at work.

Recent studies in various other world regions often have conflicting results regarding future hail occurrences. For example, modeling work suggests future decreases in CAPE in southeastern Australia under enhanced greenhouse concentrations (Niall and Walsh, 2005). However, Leslie et al. (2008) disagrees, reporting model simulations of a gradual increase in frequency and intensity of hailstorms in the Sydney Basin out to 2050. In Europe, Sanderson et al. (2015) projected a decrease in damaging hailstorms in the United Kingdom throughout the 21st century. Dessens et al. (2015) generally concur for the southern Atlantic French coast, forecasting a slight decrease in the number of hailstorms, but with no significant change in hail frequency by 2040. On the other hand, observational studies suggest that synoptic environments that favor hail precipitation have increased in the Mediterranean region (Sanchez et al., 2017) and much of central Europe (Mohr and Kunz, 2013). Bayesian modeling suggests a modest increase in the number of hail days by 2031–2045 in Germany (Kapsch et al., 2015). In the U.S., Mahoney et al. (2012) used high-resolution modeling to predict substantial decreases in hail frequency in the Colorado mountains by mid-century (2041–2070). But Allen (2017) disagreed, suggesting a potential increase in both the mean hail size and the frequency of major hailstorms in North America. Brooks (2013) summarized previous work by suggesting that CAPE can be expected to increase in the future, while wind shear will decrease, leaving the net effect

on tornado and hail occurrence in the future open to question. Again, this conclusion supports the notion that theoretical factors important to generating hail under a warming climate are in opposition.

Closer to Louisiana, Brimelow et al. (2017) used sophisticated modeling techniques to conclude that fewer days of small, medium, and large hail are expected over much of North America over the 2041–2070 period, including the U.S. Southeast and Louisiana, in spring and summer (Figure X). Figure X does suggest some possible increase in the frequency of large hail for southeastern Louisiana.

The Fourth National Climate Assessment (2017) cites Allen and Tippett (2015) in reaching the conclusion that although evidence exists for an increasing hail frequency in the U.S., the uncertainty in reported hailstone size reduces the confidence in projections (Kossin et al., 2017). Robinson (2021) cites projections by Trapp et al. (2019) of minor increases in mean number of spring hail days for much of the central and eastern U.S., counteracted by a decrease in summer hail occurrence over the eastern United States. Given the conflicting theoretical impacts of hail above, the comprehensiveness of the Brimelow et al. (2017) work, and the near certainty of an increased population to be impacted, we project 10 percent decrease in the future vulnerability to hail in Louisiana by mid-century (Mostafiz et al., 2020, 2022).

References:

Allen, J. T. (2017). Atmospheric hazards hail potential heating up. Nature Climate Change, 7, 474–475. https://doi.org/10.1038/nclimate3327

Allen, J. T. & Tippett, M. K. (2015). The characteristics of United States hail reports: 1955–2014. Electronic Journal of Severe Storms Meteorology, 10(3), 1–31. https://doi.org/10.55599/ejssm.v10i3.60

Brimelow, J. C., Burrows, W. R., & Hanesiak, J. M. (2017). The changing hail threat over North America in response to anthropogenic climate change. Nature Climate Change, 7, 516–523. https://doi.org/10.1038/nclimate3321

Brooks, H. E. (2013). Severe thunderstorms and climate change. Atmospheric Research, 123, 129–138. https://doi.org/10.1016/j.atmosres.2012.04.002

Dessens, J., Berthet, C., & Sanchez, J. L. (2015). Change in hailstone size distributions with an increase in the melting level height. Atmospheric Research, 158, 245–253. https://doi.org/10.1016/j.atmosres.2014.07.004

Kapsch, M. L., Kunz, M., Vitolo, R., & Economou, T. (2012). Long-term variability of hail-related weather types in an ensemble of regional climate models. Journal of Geophysical Research, 117, D15107. https://doi.org/10.1029/2011JD017185

Kossin, J. P., Hall, T., Knutson, T., Kunkel, K. E., Trapp, R. J., Waliser, D. E., & Wehner, M. F. (2017). Extreme storms. In: Climate Science Special Report: Fourth National Climate

Assessment, Volume I [Wuebbles, D. J., Fahey, D. W., Hibbard, K. A., Dokken, D. J., Stewart, B. C., & Maycock, T. K. (Eds.)]. U.S. Global Change Research Program, Washington, DC, USA, 257–276. https://science2017.globalchange.gov/

Leslie, L. M., Leplastrier, M., & Buckley, B. W. (2008). Estimating future trends in severe hailstorms over the Sydney Basin: A climate modelling study. Atmospheric Research, 87, 37–51. https://doi.org/10.1016/j.atmosres.2007.06.006

Mahoney, K., Alexander, M. A., Thompson, G., Barsugli, J. J., & Scott, J. D. (2012). Changes in hail and flood risk in high-resolution simulations over Colorado's mountains. Nature Climate Change, 2, 125–131. https://doi.org/10.1038/nclimate1344

Mohr, S. & Kunz, M. (2013). Recent trends and variabilities of convective parameters relevant for hail events in Germany and Europe. Atmospheric Research, 123, 211–228. https://doi.org/10.1016/j.atmosres.2012.05.016

Mostafiz, R. B., Rohli, R. V., Friedland, C. J., Gall, M., & Bushra, N. (2022). Future crop risk estimation due to drought, extreme temperature, hail, lightning, and tornado at the census tract level in Louisiana. Frontiers in Environmental Science, 10, 919782. https://doi.org/10.3389/fenvs.2022.919782

Mostafiz, R. B., Friedland, C., Rohli, R. V., Gall, M., Bushra, N., and Gilliland, J.M. (2020). Census-block-level property risk estimation due to extreme cold temperature, hail, lightning, and tornadoes in Louisiana, United States. Frontiers in Earth Science (Lausanne), 8, Art. No. 601624. https://doi.org/10.3389/feart.2020.601624

Ni, X., Zhange, Q. H., Liu, C. T., Li, X. F., Zou, T., Lin, J. P., Kong, H. I., & Ren, Z. H. (2017). Decreased hail size in China since 1980. Scientific Reports, 7, Art. No. 10913. https://doi.org/10.1038/s41598-017-11395-7

Niall, S. & Walsh, K. (2005). The impact of climate change on hailstorms in Southeastern Australia. International Journal of Climatology, 25(14), 1933–1952. https://doi.org/10.1002/joc.1233

Raupach, T. H., Martius, O., Allen, J. T., Kunz, M., Lasher-Trapp, S., Mohr, S., Rasmussen, K. L., Trapp, R. J., & Zhang, Q. (2021). The effects of climate change on hailstorms. Nature Reviews Earth & Environment, 2(3), 213–226. https://par.nsf.gov/servlets/purl/10227073

Robinson, W. A. (2021). Climate change and extreme weather: A review focusing on the continental United States. Journal of the Air & Waste Management Association, 71(10), 1186–1209. https://doi.org/10.1080/10962247.2021.1942319

Sanchez, J. L., Merino, A., Melcón, P., García-Ortega, E., Fernández-González, S., Berthet, C., & Dessens, J. (2017). Are meteorological conditions favoring hail precipitation change

in southern Europe? Analysis of the period 1948-2015. Atmospheric Research, 198, 1–10. https://doi.org/10.1016/j.atmosres.2017.08.003

Sanderson, M. G., Hand, W. H., Groenejeijer, P., Boorman, P. M., Webb, J. D. C., & McColl, L. J. (2015). Projected changes in hailstorms during the 21st century over the UK. International Journal of Climatology, 35(1), 15–24. https://doi.org/10.1002/joc.3958

Trapp, R. J., Hoogewind, K. A., & Lasher-Trapp, S. (2019). Future changes in hail occurrence in the United States determined through convection-permitting dynamical downscaling. Journal of Climate, 32(17), 5493–509. https://doi.org/10.1175/JCLI-D-18-0740.1

Xie, B., Zhang, Q., & Wang, Y. (2008). Trends in hail in China during 1960–2005. Geophysical Research Letters, 35(2008), LI 3801. https://doi.org/10.1029/2008GL034067

Xie, B., Zhang, Q., & Wang, Y. (2010). Observed characteristics of hail size in four regions in China during 1980–2005. Journal of Climate, 23(18), 4973–4982. https://doi.org/10.1175/2010JCLI3600.1

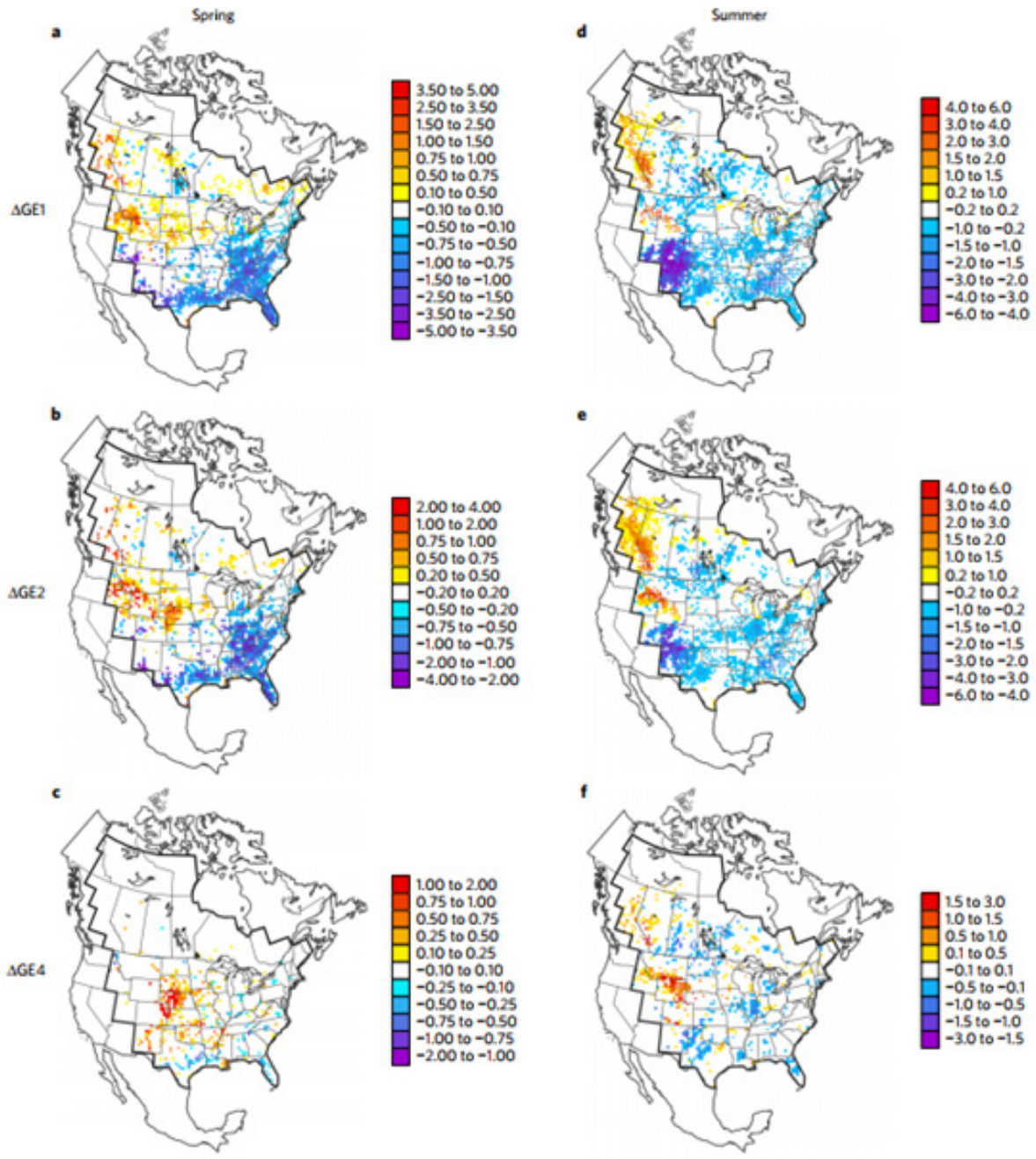

Figure 1 | Spatial changes in hail diameter classes for spring and summer. a–c, Mean multi-model changes in future (2041–2070) minus present (1971–2000) for spring hail days (GE1; $D_s \geq 1.0$ cm) per season (**a**), severe hail days (GE2; $D_s \geq 2$ cm) per season (**b**), and very large-hail days (GE4; $D_s \geq 4$ cm) per season (**c**). **d–f**, The same variables as for **a–c**, except for summer. Coloured cells indicate mean changes for all model pairings that agree on the direction of change; cells with coloured circles indicate mean changes for at least two model pairings that are statistically significant (90% significance).

Source: Verbatim from Brimelow et al. (2017)

Future Conditions: Lightning

Future changes to lightning frequency in the southern U.S. are not discussed directly in NCA4 (2017), nor is the topic covered extensively in the refereed literature. Etten-Bohm et al. (2021) note the wide range in future lightning predictions. As was described in the assessment of future conditions for high winds, there is currently low confidence in projection of severe thunderstorms. Furthermore, there is even less evidence for changes in weak to moderate thunderstorms. Because weak to moderate thunderstorms are much more frequent than severe thunderstorms, collectively they produce most of the lightning strokes. Therefore, there is very little certainty in any changes in lightning by mid-century. Recent research from China (Yang et al., 2018) suggests that future increases can be expected. For the U.S., a suite of 11 general circulation models predicted mean increases in lightning strikes for the 2079-2088 period of between 3.4% and 17.6% per °C of temperature increase (Romps et al., 2014). Yet Finney et al. (2018) projected a 15 percent global decrease in total flash rates by 2100 under RCP8.5. Based on the preponderance of evidence a 10 percent increase in the lightning hazard is assumed here for Louisiana by 2050 (Mostafiz et al., 2020, 2022).

References

Etten-Bohm, M., Yang, J., Schumacher, C., & Jun, M. (2021). Evaluating the relationship between lightning and the large-scale environment and its use for lightning prediction in global climate models. Journal of Geophysical Research: Atmospheres, 126(5), e2020JD033990. https://doi.org/10.1029/2020JD033990

Finney, D. L., Doherty, R. M., Wild, O., Stevenson, D. S., MacKenzie, I. A., & Blyth, A. M. (2018). A projected decrease in lightning under climate change. Nature Climate Change, 8(3), 210–213. https://doi.org/10.1038/s41558-018-0072-6

Mostafiz, R. B., Rohli, R. V., Friedland, C. J., Gall, M., & Bushra, N. (2022). Future crop risk estimation due to drought, extreme temperature, hail, lightning, and tornado at the census tract level in Louisiana. Frontiers in Environmental Science, 10, 919782. https://doi.org/10.3389/fenvs.2022.919782

Mostafiz, R. B., Friedland, C., Rohli, R. V., Gall, M., Bushra, N., and Gilliland, J.M. (2020). Census-block-level property risk estimation due to extreme cold temperature, hail, lightning, and tornadoes in Louisiana, United States. Frontiers in Earth Science (Lausanne), 8, Art. No. 601624. https://10.3389/feart.2020.601624

Romps, D. M., Seeley, J. T., Vollaro, D., & Molinari, J. (2014). Projected increase in lightning strikes in the United States due to global warming. Science, 346(6211), 851–854. https://doi.org/10.1126./science.1259100

Yang, Y. R., Song, D., Wang, S. Y., Li, P., & Xu, Y. (2018). Characteristics of cloud-to-ground lightning and its relationship with climate change in Muli, Sichuan province, China. Natural Hazards, 91, 1097–1112. https://doi.org/10.1007/s11069-018-3169-3

Future Conditions: Tornadoes

The updraft of air in tornadoes always rotates because of wind shear (differing horizontal speed height), and it can rotate in either a clockwise or counterclockwise direction. Clockwise rotations (in the northern hemisphere) will always result in near-immediate demise, but counterclockwise rotations (in the northern hemisphere) will sustain the system, at least until other forces cause it to die seconds to minutes later.

The Enhanced Fujita (EF) Scale is used to classify tornadoes based on their damage pattern, not wind speed; wind speed is then derived and estimated. This contrasts with the Saffir-Simpson scale used for hurricane classification, which is based on measured wind speed.

Enhanced Fujita (EF) Scale.

ENHANCED FUJITA SCALE						
	EF0	EF1	EF2	EF3	EF4	EF5
Wind Speed	65-85 mph	86-110 mph	111-135 mph	136-165 mph	166-200 mph	>200 mph

Any estimates on changing tornado frequencies or intensities should begin with an assessment of the likelihood of changing precursor conditions for tornadoes. Increases in the frequency of convergence of very warm, humid air masses with very cold air masses and/or increases in the intensity of the temperature gradient across air masses would be likely to increase the tornado frequency and/or intensity, and therefore presumably increase vulnerability to tornadoes. Likewise, increasing vertical temperature gradients between the surface and aloft (i.e. more rapid decreases in temperature with increasing height) would also make tornadoes stronger and/or more likely, and therefore exacerbate tornado vulnerability. A related ingredient is vertical wind shear (i.e., sharp increases in wind speed with increasing height), with increasing vertical wind shear over time promoting increasing situations of the horizontal rotation that could then be raised to a vertically oriented rotating mass if warming air near the surface increases the tendency for it to rise. Increases in tropical cyclone frequency would also be likely to increase the number of tropical cyclone-induced tornadoes, and presumably tornado vulnerability. And finally, enhancements in detection capabilities and increasing population generally would increase the number of reported tornadoes, particularly weaker ones.

There remains a general lack of consensus regarding the impact of global climatic change on tornado frequency and/or intensity (Long and Stoy, 2014). Part of the difficulty in making such projections is the large difference in scale between global climate change projections and the local nature of the weather conditions that create tornadoes (Mika, 2013), along with an incomplete understanding of the physics involved (Moore et al., 2015). Nevertheless, the existing scientific literature can give at least some basis for assessing tornado vulnerability regarding the scenarios described in the previous paragraph.

Atmospheric scientists overwhelmingly agree that global temperatures will continue increasing, though the magnitude and rate of increase will vary spatially, seasonally, and within the diurnal cycle (National Climate Assessment, *2017; https://science2017.globalchange.gov).*

As was discussed, temperature is expected to increase in Louisiana at least through mid-century. Increasing temperatures would logically move the boundary between the cold and warm air masses poleward, leaving Louisiana farther from the most dangerous zone for tornadic development a larger percentage of the time, and therefore reduce tornado frequency and/or intensity. Because tornado frequency in Louisiana is less seasonal than in most other places, the nuances of changing tornado vulnerability may be slightly less dependent on the uncertainties of the seasonal temperature changes than in most other places.

However, the other factors that also impact tornado frequencies must also be considered. As suggested above, tornadic activity is also favored when very warm, humid air near the surface underlies air that is much colder aloft. Thus, amplification of the temperature difference between the surface and the upper atmosphere (i.e., destabilizing the atmosphere) might be considered to enhance the probability of tornadic development. Brooks (2013) used climate model simulations to conclude that indeed, that vertical gradient, as represented by convective available potential energy (CAPE), is projected to increase into the future. However, Brooks (2013) also noted that the vertical wind shear needed for tornadic development is generally weakening under global change climate simulations. Gensini et al. (2014) noted using a regional model simulation that extreme destabilization of the atmosphere (in the form of the number of days having an extremely high CAPE) is likely to increase over a large section of the northeastern U.S.A., which would make tornadoes more likely. However, the same study showed that CAPE is likely to decrease over nearly all of Louisiana, at least when the 2041–2065 period is compared to the 1981–1995 interval, which would create a less favorable environment for tornadoes.

On the other hand, Diffenbaugh et al. (2013) disagreed, noting that the days with weakening vertical wind shear tend to be concentrated on days when CAPE is low; with high-CAPE days showing less evidence of weakening shear. Seeley and Romps (2015) generally concurred with Diffenbaugh et al. (2013), excepting that their analysis was for severe thunderstorms rather than tornadoes per se. Through ensemble modeling, Seeley and Romps (2015) found consistent spring and summer increases in the frequency of severe-thunderstorm environments over the U.S., including Louisiana, from 2079-2088, as represented by high CAPE days and vertical wind shear, under medium and high scenarios of greenhouse forcing.

Furthermore, tornadic development also occurs in association with tropical cyclones, so any changes in tropical cyclone frequency and/or intensity might coincide with a change in tropical-cyclone-induced tornadic development. As previously discussed, tropical cyclones are expected to become more problematic in the future, even if only because of increased coastal population. Therefore, in the absence of prevailing scientific consensus on the topic in the refereed literature, it seems reasonable to suggest that the tropical-

cyclone-induced tornado hazard will follow a proportionate increase to that of tropical cyclones for Louisiana, with the caveat that as tornado detection capabilities continue to improve due to larger populations and improved equipment to observe their occurrence, the percentage of tornado frequencies that are reported is expected to increase.

When comparing the 1954–1983 period to the 1984–2013 period, Agee et al. (2016) found that, not surprisingly, winter was the season in which the most prominent tornado frequency increases occurred. For Louisiana, that study showed an increase in the latter period in EF5 tornadoes. However, Louisiana experienced a simultaneous decrease in the number of days on which a tornado occurred (Agee et al., 2016), which suggests that tornado outbreaks may be becoming more frequent, even while tornado frequencies are not. Tippett et al. (2016) concurred, suggesting that increases in larger outbreaks will be more pronounced than increases in smaller outbreaks. And importantly, NCA4 (2017) agrees that the frequency of tornado days in the U.S. has decreased since 1970, but that the number of tornadoes touching down on those days has increased over the same time period (Kossin et al., 2017). The latter study also reports an earlier onset of tornado season in the United States.

Modeling studies of future tornadic activity reveal a mixed bag. Trapp and Hoogewind (2016) found that updrafts, while intense under projected increases in CAPE by the latter 21st century, do not increase proportionately to the projected CAPE. Kossin et al. (2017) agree in NCA4, as historical tornado outbreaks such as the Joplin, Missouri, tornadoes of 2011 do not become even more severe when placed in an environment of CAPE by the late 21st century, but nor do such outbreaks break apart either.

As coastal population increases and temperature rises, the destabilization in the atmosphere could result in more frequent tornado outbreaks, which would occur when abundant vertical wind shear is present over Louisiana and/or in the presence of a tropical cyclone. However, the literature is uncertain on whether the windows of time in which these conditions are met may change. And the impacts due to increased vulnerabilities may outstrip the increasing tornado frequencies in the future (Strader et al., 2017). All these factors lead us to estimate an increase in Louisiana tornadoes by 10 percent by 2050 (Mostafiz et al., 2020, 2022), despite a likely relatively constant frequency in the most reliable portions of the climatological record (Gensini, 2021).

References

Agee, E., Larson, J., Childs, S., Marmo, A. (2016). Spatial redistribution of U.S. tornado activity between 1954 and 2013. Journal of Applied Meteorology and Climatology, 55(8), 1681–1697. https://www.jstor.org/stable/e26179792

Brooks, H. E. (2013). Severe thunderstorms and climate change. Atmospheric Research, 123, 129–138. https://doi.org/10.1016/j.atmosres.2012.04.002

Diffenbaugh, N. S., Scherer, M., & Trapp, R. J. (2013). Robust increases in severe thunderstorm environments in response to greenhouse forcing. Proceedings of the National Academy of Sciences of the United States of America, 110(41), 16361–16366. https://doi.org/10.1073/pnas.1307758110

Gensini, V. V. A. (2021). Severe convective storms in a changing climate. In Fares, A. (Ed.), Climate Change and Extreme Events (pp. 39-56). Elsevier. 978-0128227008

Kossin, J. P., Hall, T., Knutson, T., Kunkel, K. E., Trapp, R. J., Walisre, D. E., & Wehner, M. F. (2017). Extreme storms. In: Climate Science Special Report: Fourth National Climate Assessment, Volume I [Wuebbles, D. J., Fahey, D. W., Hibbard, K. A., Dokken, D. J., Stewart, B. C., & Maycock, T. K. (Eds.)]. U.S. Global Change Research Program, Washington, DC, USA, pp. 257–276. https://science2017.globalchange.gov/

Long, J. A. & Stoy, P. C. (2014). Peak tornado activity is occurring earlier in the heart of "Tornado Alley." Geophysical Research Letters, 41(17), 6259–6264. https://doi.org/10.1002/2014GL061385

Mika, J. (2013). Changes in weather and climate extremes: Phenomenology and empirical approaches. Climatic Change, 121(1), 15–26. https://doi.org/10.1007/s10584-013-0914-1

Moore, T. R., Matthews, H. D., Simmons, C., & Leduc, M. (2015). Quantifying changes in extreme weather events in response to warmer global temperature. Atmosphere-Ocean, 53(4), 412–425. https://doi.org/10.1080/07055900.2015.1077099

Mostafiz, R. B., Rohli, R. V., Friedland, C. J., Gall, M., & Bushra, N. (2022). Future crop risk estimation due to drought, extreme temperature, hail, lightning, and tornado at the census tract level in Louisiana. Frontiers in Environmental Science, 10, 919782. https://doi.org/10.3389/fenvs.2022.919782

Mostafiz, R. B., Friedland, C., Rohli, R. V., Gall, M., Bushra, N., and Gilliland, J.M. (2020). Census-block-level property risk estimation due to extreme cold temperature, hail, lightning, and tornadoes in Louisiana, United States. Frontiers in Earth Science (Lausanne), 8, Art. No. 601624. https://doi.org/10.3389/feart.2020.601624

Seeley, J. T. & Romps, D. M. (2015). The effect of global warming on severe thunderstorms in the United States. Journal of Climate, 28(6), 2443–2458. https://doi.org/10.1175/JCLI-D-14-00382.1

Strader, S. M., Ashley, W. S., Pingel, T. J., & Krmenec, A. J. (2017). Projected 21st century changes in tornado exposure, risk, and disaster potential. Climatic Change, 141, 301–313. https://doi.org/10.1007/s10584-017-1905-4

Tippett, M. K., Lepore, C. & Cohen, J. E. (2016). More tornadoes in the most extreme U.S. tornado outbreaks. Science, 354(6318), 1419–1423. https://doi.org/10.1126/science.aah7393

Trapp, R. J. & Hoogewind, K. A. (2016). The realization of extreme tornadic storm events under future anthropogenic climate change. Journal of Climate, 29(14), 5251–5265. https://doi.org/10.1175/JCLI-D-15-0623.1

Future Conditions: Floods

As noted in NCA4 (2017), projection of the flood hazard to 2050 is a complex multivariate problem, as human activities such as deforestation, urban development, construction of dams, flood mitigation measures, and changes in agricultural practices impact future flood statistics. In addition, Louisiana's geography superimposes such local-to-regional-scale changes on similar changes upstream over a significant portion of the nation, and these changes are superimposed on climatic changes and eustatic sea level rise.

Despite these complications inviting caution in the interpretation of results, it is safe to conclude that flooding is likely to remain Louisiana's costliest, most ubiquitous, and most life-threatening hazard. This is because floods are the by-product of several other hazards profiled earlier in this report, including thunderstorms, tropical cyclones, coastal hazards, dam failure, and levee failure. The "future conditions" sections of those hazards (presented earlier in this report) projected changes in vulnerability as summarized in Table X below.

Table X. Estimated change in future vulnerability in Louisiana by 2050, by hazard

Hazard	Estimated Change in Future Vulnerability by 2050 (%)
Severe thunderstorms	+10
Tropical cyclones	+25
Coastal hazards	"High"
Dam failure	0
Levee failure	0

Based on the information summarized in Table X, there is no reason to expect that the flood hazard in Louisiana will abate, particularly as population increases. We fully support the use of Louisiana's Comprehensive Master Plan for a Sustainable Coast in planning for the future flood hazard.

However, the news is not all dire, nor is the situation hopeless. By some accounts, the rate of coastal land loss has shown some signs of slowing. Renewed commitment to smart-growth strategies, especially in floodplains, levee-protected areas, and in the area vulnerable to direct inundation from storm surge or meteotsunami, will mitigate future flood disasters. These strategies include, but are not limited to, the "multiple lines of defense" approach (Lopez, 2009) and effective implementation of recommendations in

Louisiana's Comprehensive Master Plan for a Sustainable Coast (Coastal Protection and Restoration Authority of Louisiana, 2017, 2023). And there are several effective examples of environmental challenges that have been mitigated through public awareness/education, and mutual resolve (e.g., ozone hole, oil spills, nuclear power plant meltdowns, etc.). While the flooding hazard in Louisiana will never be eliminated, it is possible that we can coexist sustainably alongside the hazard.

References:

Ashley, S. T. & Ashley, W. S. (2008). Flood fatalities in the United States. Journal of Applied Meteorology and Climatology, 47(3), 805–818. https://doi.org/10.1175/2007JAMC1611.1

Coastal Protection and Restoration Authority of Louisiana. (2017). Louisiana's Comprehensive Master Plan for a Sustainable Coast. Baton Rouge, LA. https://coastal.la.gov/reports/2017-coastal-master-plan/

Coastal Protection and Restoration Authority of Louisiana. (2023). Louisiana's Comprehensive Master Plan for a Sustainable Coast. Baton Rouge, LA. https://coastal.la.gov/our-plan/2023-coastal-master-plan/

Lopez, J. A. (2009). The multiple lines of defense strategy to sustain coastal Louisiana. Journal of Coastal Research, 54, 186–197. https://doi.org/10.2112/SI54-020.1

Future Conditions: Dam Failures

Even if extreme precipitation events would increase in frequency and/or magnitude in the future and earthquake probability increases, there is no evidence to suggest that future conditions would contribute to an enhanced likelihood of dam failures due to natural causes. As the dams are designed to standards, this should already be contemplated in the design guidance. The anthropogenic component of the dam failure hazard is beyond the scope of this analysis. Therefore, despite anticipated increases in other natural hazards, there is no indication that these increases will result in additional dam failures, at least from a natural hazard perspective.

Future Conditions: Levee Failures

Any assessment of the future conditions relating to levee failures in Louisiana must begin with an assessment of the future conditions relative to the natural hazards that would most likely cause the levees to fail. These hazards include tropical cyclones (including storm surge), flooding, and earthquakes. Earlier reports in this document have assessed each of these hazards as likely to increase in the future.

Possible opposing forces that might mitigate the levee hazard include smart growth, lessons learned from the Katrina levee failures, new science and technology, and improved engineering.

To calculate the current probability of failure, it is conservatively assumed that 2,000 distinct levee breaches have occurred nationally in the past 25 years. This figure includes The Great Flood of 1993, where Mississippi River levees were overtopped or breached in over 1,000 locations, and Hurricane Katrina in 2005, where 50 levee breaches were reported to have occurred. Assuming 1 mile between distinct breaches and the 22,950 miles of levees in the U.S. (https://levees.sec.usace.army.mil/#/), the probability of failure within one mile of levee is calculated as:

$$\frac{2{,}000 \text{ breaches}}{22{,}950 \text{ miles of levees}} \Big/ {}_{25 \text{ years}} = 0.3\% \text{ annual probability}$$

But because the previous occurrences for this hazard are rare, the increased hazard in the future will be minimal.

There are no future conditions related to the levees themselves that would enhance the probability of levee failures due to natural causes. Design guidance and oversight in the future should ensure that the levees are designed to standards. Therefore, even though we anticipate increases in rainfall and earthquake hazards, there is no indication that these increases will result in additional levee failures.

Geologic Hazards

Earthquake

Earthquakes are typically described in terms of magnitude and intensity. Magnitude is the measure of the amplitude of the seismic wave and is often expressed by the Richter scale. The Richter scale is a logarithmic measurement, whereby an increase in the scale by one whole number represents a tenfold increase in measured ground motion of the earthquake (and a more than thirty-fold increase in energy released). An increase by two whole numbers represents a 102 (or 100-fold) increase in ground motion, and thus more than 302 (or 900) times the energy released. Intensity is a measure of how strongly the shock was felt at a particular location, indexed by the Modified Mercalli Intensity (MMI) scale.

A fault Is a fracture in the Earth's crust where movement occurs on one side relative to the other. Known faults in Louisiana are often caused by subsidence. The system of subsidence faults in southern Louisiana developed due to accelerated land subsidence and rapid sediment deposition from the Mississippi River. The system stretches across the southern portion of the state from Beauregard Parish in the west to St. Tammany Parish in the east,

including every parish south of this line. This system is thought to be responsible for many of the recorded earthquakes from 1843 to the present. All earthquakes that occurred over this period were of low magnitude, resulting mostly in limited property damage (such as broken windows, damaged chimneys, and cracked plaster).

Future Conditions: Earthquakes

Earthquakes are considered by most to be among the least ominous hazards in Louisiana's future. However, there are several indications that the hazard in Louisiana is likely to increase in the future. First, wastewater injection into deep wells, oil and gas exploration, and hydraulic fracturing ("fracking") are believed to be contributing to a sudden increase in earthquake activity, especially in the oil and gas mining areas, with such activities showing no signs of decrease in the near future. In the most comprehensive recent research on the earthquake hazard for the central and eastern U.S., Petersen et al. (2016) found that seismicity has increased by up to one order of magnitude over the last decade in some oil and gas-producing areas. While Petersen et al. (2016) found no induced earthquakes reported in Louisiana over the 2014–2015 period, several earthquakes associated with wells were reported in nearby adjacent Arkansas and Texas (Figure X.Y). Walter et al. (2016) suggested that seismicity is increasing in northwestern Louisiana in response to energy extraction activities. Second, Louisiana lies sufficiently near the New Madrid fault to be impacted by future movement, as it was during the series of quakes from 1811 to 1812. Page and Hough (2014) found no evidence to suggest that the seismicity associated with this fault is decaying with time. Increasing development over time would make any impacts to the Mississippi River, including but not limited to a catastrophic change of its course as happened in 1811–1812, catastrophic. These impacts could trigger a levee failure. And third, the continuing lax building codes for mitigating earthquake damage invites additional concern for an increased future vulnerability to this hazard. If anything, elevation of structures to mitigate the flood, storm surge, rising sea level, and tropical cyclone hazards might increase vulnerability to damage from non-Mississippi-River-impacted earthquakes.

For these reasons, the team assessed the future conditions relative to the earthquake hazard over the next thirty years as increasing by 10 percent.

References:

Page, M. T. & Hough, S. E. (2014). The New Madrid seismic zone: Not dead yet. Science, 343(6172), 762–764. https://doi.org/10.1126/science.1248215

Petersen, M. D., Mueller, C. S., Moschetti, M. P., Hoover, S. M., Llenos, A. L., Ellsworth, W. L., Michael, A. J., Rubinstein, J. L., McGarr, A. F., & Rukstales, K. S. (2016). Seismic-hazard forecast for 2016 including induced and natural earthquakes in the central and eastern United States. Seismological Research Letters, 87, 1327–1341. https://www.usgs.gov/publications/seismic-hazard-forecast-2016-including-induced-and-natural-earthquakes-central-and

Walter, J. I., Dotray, P. J., Frohlich, C., & Gale, J. F. W. (2016). Earthquakes in northwest Louisiana and the Texas-Louisiana border possibly induced by energy resource activities within the Haynesville shale play. Seismological Research Letters, 87(2A), 285–294. https://doi.org/10.1785/0220150193

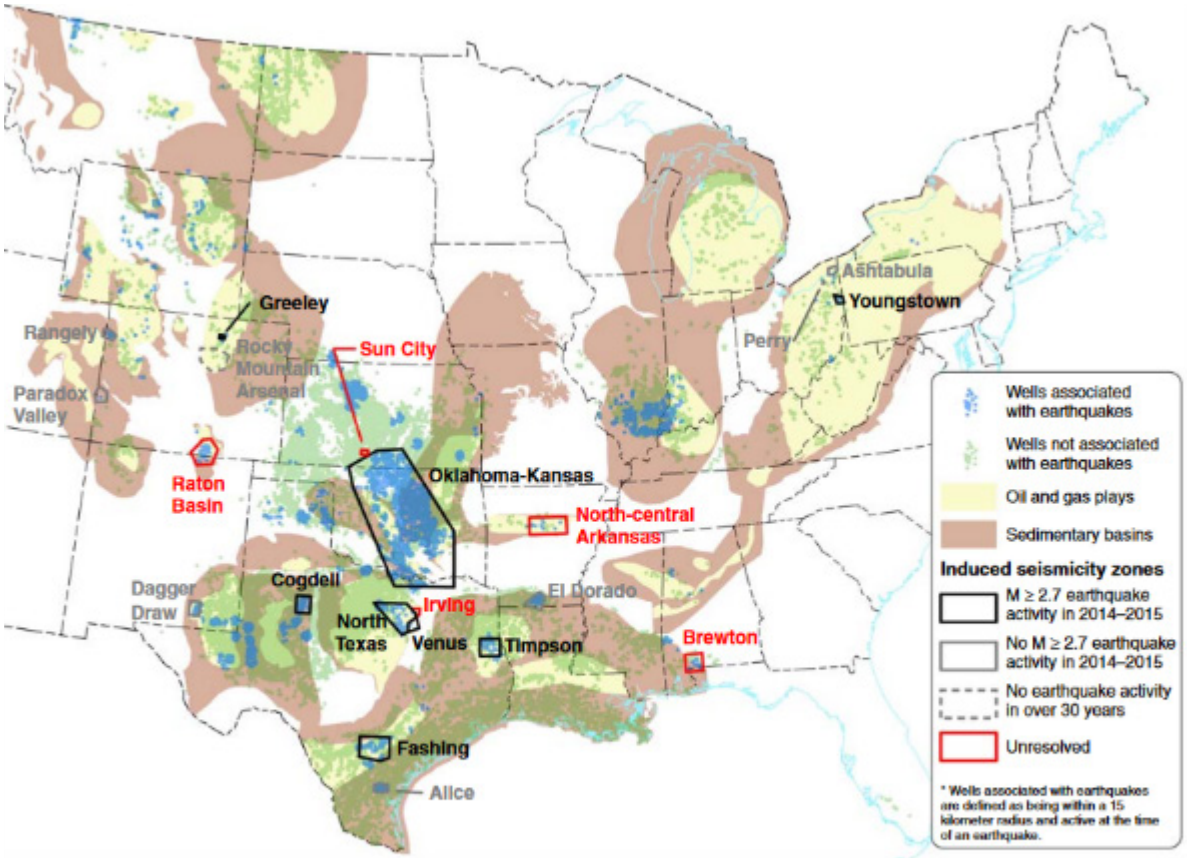

▲ **Figure 1.** Zones of induced seismicity defined in this report. Additional details about the zones are provided in Table 1. Information on oil and gas plays, sedimentary basins (U.S. Energy Information Administration, 2015), wells that are associated with earthquakes (Weingarten *et al.*, 2015), and the earthquake zones applied in this analysis. (Figure from Petersen *et al.*, 2016). The color version of this figure is available only in the electronic edition.

Future Conditions: Sinkholes

The geological bedrock and regolith underlying Louisiana will not change on human timescales, and the relatively small percentage of Louisiana's land area composed of carbonate bedrock points to a small hazard related to karst-induced sinkholes. Nevertheless, Autin (2002) emphasizes that uplift of the Five Islands of southwestern Louisiana is probably still active, leaving tectonic and geomorphic instability possible in the future. The hazard relative to sinkholes could change much more rapidly with land use change and the pressures of increased resource extraction and population growth. Vulnerability to sinkholes could also increase as a "side effect" to changes in the vulnerability to in other hazards. Neal (2020) expressed the concern that sinkhole-related mining accidents along the storage facilities for the U.S. National Petroleum Reserve, which is along the Louisiana and Texas coasts, could endanger national interests.

Furthermore, sea level rise contributes to saltwater intrusion, which contributes to the formation of salt domes, which—when mined extensively—can form sinkholes.

Even though geological changes are unlikely, other environmental modifications are connected with changes in sinkhole formation, including, according to Demir and Keskin (2020), anthropogenic effects. Nevertheless, it is important to note that geological factors such as groundwater leakage rates (i.e., Xiao and Li 2020) may also be important indicators of sinkhole formation, independent of climate change considerations. Sedimentation in sinkholes has also been used as an indicator of climate and sea level change (Hodell et al., 2005; van Hengstum et al., 2011; Kovacs et al., 2013; Gregory et al., 2017; Peros et al., 2017; Farley et al., 2018). Taminskas and Marcinkevicius (2002) pointed out that climate change may drive karstification that then in turn affects sinkhole formation. Panno et al. (2012) noticed that cave formation was affected by climate change in the Pleistocene. Linares et al. (2017) found that drought facilitates sinkhole formation in some karst settings, including northeastern Spain. Most recently, biological manifestations of climate change in sinkholes have been shown for vascular plants (Bátori et al., 2014; Kiss et al., 2020), bryophytes (Liu et al., 2019), and forests (Yang et al., 2019).

In light of the above factors, the annual probability estimate for areas overlying a salt dome is likely to increase somewhat by 2050. This is due to likely increasing population (and therefore, it is assumed, groundwater pumping) and human activities (including resource extraction, possibly from hydraulic fracture drilling), along with the destabilizing effects of global and regional sea level rise on coastal salt domes, are increasingly likely to generate additional accidental events. Considering these considerations, we project a 50 percent increase in the state's sinkhole hazard by 2050.

Sinkhole Risk Assessment:

Property loss due to sinkhole is calculated as

$$PL_{2050,i} = SL_{2050,i} + CL_{2050,i}$$

$$SL_{2050,i} = (SV_{2050,i} \times A_i \times H_{historical} \times F_{2050})[R \times L_A + (1 - R) \times L_B]$$

$$CL_{2050,i} = CV_{2050,i} \times A_i \times H_{historical} \times F_{2050} \times R \times L_A$$

where

$PL_{2050,i}$ = projected annual preperty loss of census block i in 2050
$SL_{2050,i}$ = annual building/structure loss of census block i in 2050
$CL_{2050,i}$ = annual content loss of census block i in 2050
$SV_{2050,i}$ = building/structure value of census block i in 2050
$CV_{2050,i}$ = content value of census block i in 2050
A_i = percentage of area of census block i under saltdomes
$H_{historical}$ = historical hazard intensity
F_{2050} = hazard intensity in 2050
R = ratio between largest sinkholes to largest salt domes
L_A = 100 percent loss of SV and CV
L_B = 50 percent loss of SV

We consider the ratio of largest sinkhole incident area in Louisiana (although there were only two incidents) to the largest salt dome area to calculate the losses. Caution should be exercised in the interpretation of results because identification of which portion/part of salt domes will turn into sinkholes is highly uncertain.

References

Autin, W. J. (2002). Landscape evolution of the Five Islands of south Louisiana: Scientific policy and salt dome utilization and management. Geomorphology, 47(2–4), 227–244. https://doi.org/10.1016/S0169-555X(02)00086-7

Bátori, Z., Csiky, J., Farkas, T., Vojtkó, E. A., Erdős, L., Kovács, D., Wirth, T., Körmöczi, L., and Vojtkó, A. (2014). The conservation value of karst dolines for vascular plants in woodland habitats of Hungary: refugia and climate change. International Journal of Speleology, 43(1), 15–26. https://doi.org/10.5038/1827-806X.43.1.2

Demir, V., and Keskin, A. Ü. (2020). Water level change of lakes and sinkholes in Central Turkey under anthropogenic effects. Theoretical and Applied Climatology, 142(3), 929–943. https://doi.org/10.1007/s00704-020-03347-5

Farley, G., Schneider, L., Clark, G., and Haberle, S. G. (2018). A Late Holocene palaeoenvironmental reconstruction of Ulong Island, Palau, from starch grain, charcoal, and geochemistry analyses. Journal of Archaeological Science: Reports, 22, 248–256. https://doi.org/10.1016/j.jasrep.2018.09.024
Gregory, B. R., Reinhardt, E. G., and Gifford, J. A. (2017). The influence of morphology on sinkhole sedimentation at Little Salt Spring, Florida. Journal of Coastal Research, 33(2), 359–371. https://doi.org/10.2112/JCOASTRES-D-15-00169.1

Hodell, D. A., Brenner, M., Curtis, J. H., Medina-Gonzalez, R., Can, E. I. C., Albornaz-Pat, A., and Guilderson, T. P. (2005). Climate change on the Yucatan Peninsula during the little ice age. Quaternary Research, 63(2), 109–121. https://doi.org/10.1016/j.yqres.2004.11.004

Kiss, P. J., Tölgyesi, C., Bóni, I., Erdős, L., Vojtkó, A., Maák, I. E., and Bátori, Z. (2020). The effects of intensive logging on the capacity of karst dolines to provide potential microrefugia for cool-adapted plants. Acta geographica Slovenica, 60(1), 37–48. https://doi.org/10.3986/AGS.6817

Kovacs, S. E., van Hengstum, P. J., Reinhardt, E. G., Donnelly, J. P., and Albury, N. A. (2013). Late Holocene sedimentation and hydrologic development in a shallow coastal sinkhole on Great Abaco Island, The Bahamas. Quaternary International, 317, 118–132. https://doi.org/10.1016/j.quaint.2013.09.032

Linares, R., Roqué, C., Gutiérrez, F., Zarroca, M., Carbonel, D., Bach, J., and Fabregat, I. (2017). The impact of droughts and climate change on sinkhole occurrence. A case study from the evaporite karst of the Fluvia Valley, NE Spain. Science of the Total Environment, 579(2017),

345–358. https://doi.org/10.1016/j.scitotenv.2016.11.091

Liu, R., Zhang, Z., Shen, J., and Wang, Z. (2019). Bryophyte diversity in karst sinkholes affected by different degrees of human disturbance. Acta Societatis Botanicorum Poloniae, 88(2), Art. No. 3620. https://doi.org/10.5586/asbp.3620

Mostafiz, R. B., Friedland, C. J., Rohli, R. V., & Bushra, N. (2021). Property risk assessment of sinkhole hazard in Louisiana, U.S.A. Frontiers in Environmental Science, 9, Art. No. 780870. https://doi.og/10.3389/fenvs.2021.780870

Neal, J. T. (2020). Mine-induced sinkholes over the US Strategic Petroleum Reserve (SPR) storage facility at Weeks Island, Louisiana: Geologic mitigation and environmental monitoring. In The Engineering Geology and Hydrology of Karst Terrains (pp. 357–361). CRC Press.

Panno, S. V., Curry, B. B., Wang, H., Hackley, K. C., Zhang, Z., and Lundstrom, C. C. (2012). The effects of climate change on speleogenesis and karstification since the penultimate glaciation in southwestern Illinois' sinkhole plain. Carbonates and Evaporites, 27(1), 87–94. https://doi.org/10.1007/s13146-012-0086-5

Peros, M., Collins, S., G'Meiner, A. A., Reinhardt, E., and Pupo, F. M. (2017). Multistage 8.2 kyr event revealed through high- resolution XRF core scanning of Cuban sinkhole sediments. Geophysical Research Letters, 44(14), 7374–7381. https://doi.org/10.1002/2017GL074369
Taminskas, J., and Marcinkevicius, V. (2002). Karst geoindicators of environmental change: The case of Lithuania. Environmental Geology, 42(7), 757–766. https://doi.org/10.1007/s00254-002-0553-8

van Hengstum, P. J., Scott, D. B., Gröcke, D. R., and Charette, M. A. (2011). Sea level controls sedimentation and environments in coastal caves and sinkholes. Marine Geology, 286(1–4), 35–50. https://doi.org/10.1016/j.margeo.2011.05.004

Xiao, H., and Li, H. (2020). Modeling downward groundwater leakage rate to evaluate the relative probability of sinkhole development at an under-construction expressway and its vicinity. Frontiers in Earth Science, 8, Art. No. 225. https://doi.org/10.3389/feart.2020.00225
Yang, G., Peng, C., Liu, Y., and Dong, F. (2019). Tiankeng: An ideal place for climate warming research on forest ecosystems. Environmental Earth Sciences, 78(2), Art. No. 46. https://doi.org/10.1007/s12665-018-8033-y

Future Conditions: Expansive Soil

The soil structure will remain largely unchanged on anthropogenic time scales. However, long-term changes in the freeze-thaw climatology and/or precipitation climatology could impact the stability of the soil structure for supporting construction (Tabassum and Bulut, 2023). The anticipated decrease in number of freezing-temperature days as

temperature increases (Vose et al., 2017; their Figure 6.9), at least under the highest-CO2-emission scenario, would diminish the future expansive soil hazard due to a decrease in freeze-thaw expansion/contraction. However, the likelihood of an increasing number of extreme hot days (Vose et al., 2017; their Figure 6.9) and heavier precipitation by 2050 interrupted by lengthening dry periods (Wehner et al., 2017), albeit again under the highest-CO2-emission scenario, may overcompensate, causing a net increase expansion/contraction. The net effect of these forces leads to a projection of an increase in the expansive soil hazard of 15 percent by 2050 (Mostafiz et al., 2021).

Expansive Soil Risk Assessment:

Property loss due to expansive soil is calculated as

$$PL_{2050,i} = SP_i \times F \times I_{2020,i} \times \frac{P_{2050,i}}{P_{2020,i}} \times \frac{MC}{R}$$

where

$PL_{2050,i}$ = projected annual property loss of census block i in 2050
SP_i = average swelling potentiality of census block i
F = future hazard multiplication factor in 2050
$I_{2020,i}$ = total building inventory value of census block i in 2020
$P_{2050,i}$ = projected population of census block i in 2050
$P_{2020,i}$ = population of census block i in 2020
MC = maintainance cost of building against the expansive soils during its useful life span
R = average life span of a residential building

Wang's (2016) point-based SP was mapped based on data measured by Seed et al. (1962).

Mostafiz, R. B., Friedland, C. J., Rohli, R. V., Bushra, N., & Held, C. L. (2021). Property risk assessment for expansive soils in Louisiana. Frontiers in Built Environment, 7, Art. No. 754761. https://doi.org/10.3389/fbuil.2021.754761

Seed, H. B., Woodward, R. J., & Lundgren, R. (1962). Prediction of swelling potential for compacted clays. Journal of the Soil Mechanics and Foundations Division, 88(3), 53–88. https://doi.org/10.1061/JSFEAQ.0000431

Tabassum, N., & Bulut, R. (2023). Residential house foundations on expansive soils in changing climates. Cityscape, 25(1), 199–212.

Vose, R. S., Easterling, D. R., Kunkel, K. E., LeGrande, A. N., and Wehner, M. F. (2017). Temperature changes in the United States. In: Climate Science Special Report: Fourth National Climate Assessment, Volume I [Wuebbles, D. J., Fahey, D. W., Hibbard, K. A., Dokken, D. J., Stewart, B. C., & Maycock, T. K. (Eds.)]. U.S. Global Change Research Program, Washington, DC, USA, pp. 185–206, https://10.7930/J0N29V45

Wang, J. X. (2016). Expansive soils and practice in foundation engineering. A presentation delivered at the 2016 Louisiana Transportation Conference 03/07/2016. http://www.ltrc.lsu.edu/ltc_16/pdf/presentations/10-University%20Transportation%20Centers%20(Part%201)-Characterization%20of%20Expansive%20Soils%20in%20Northern%20Louisiana.pdf